Available online at www.sciencedirect.com
SCIENCE DIRECT®
Journal of Magnetic Resonance 167 (2004) 185–210
JMR Journal of Magnetic Resonance
www.elsevier.com/locate/jmr

Minimum energy pulse synthesis via the inverse scattering transform

Charles L. Epstein[1]

LSNI, Department of Radiology, HUP, USA
Department of Mathematics, University of Pennsylvania, Philadelphia, PA 19104-6395, USA

Received 21 January 2003; revised 30 December 2003

Abstract

This paper considers a variety of problems in the design of selective RF-pulses. We apply a formula of Zakharov and Manakov to directly relate the energy of an RF-envelope to the magnetization profile and certain auxiliary parameters used in the inverse scattering transform (IST) approach to RF-pulse synthesis. This allows a determination of the minimum possible energy for a given magnetization profile. We give an algorithm to construct both the minimum energy RF-envelope as well as any other envelope that produces a given magnetization profile. This includes an algorithm for solving the Gel'fand–Levitan–Marchenko equations with bound states. The SLR method is analyzed in terms of traditional scattering data, and shown to be a special (singular) case of the IST approach. RF-envelopes are computed for a variety of examples.

Keywords: Nuclear magnetic resonance; Imaging; RF-pulse synthesis; Selective excitation; Inverse scattering; Marchenko equation; Minimum energy; Bound states

1. Introduction

The synthesis or design of RF-pulse sequences to produce selective excitations is a problem of central importance in all applications of nuclear magnetic resonance. The oldest systematic method of pulse synthesis is the *Fourier transform* method. Notwithstanding the fact that this method is an approximation for all non-zero flip angles, it gives usable results for flip angles up to about $\pi/2$. Over the past 20 years, more exact and systematic approaches to solving this problem have been introduced and explored. The *Shinnar–Le Roux* or *SLR* algorithm was discovered independently by Shinnar et al. and Le Roux. See for example [20,21] or [10]. A more complete list of the original papers can be found in the references to [14]. A second method is to use an *inverse scattering transform* or *IST*. There are, in fact, two different IST approaches to pulse design. An earlier method employing a reduction of the Bloch equation to a scalar Schrödinger equation appears, for example in [8,9,23–25]. Later it was realized that the IST for the spin-domain Bloch equation could be used directly, see [4,5,17]. In a sense, made precise in Section 8, the SLR is, in part, a special case of the inverse scattering transform for the spin-domain Bloch equation. A thorough discussion of methods used to design RF-pulses, prior to the introduction of the SLR and the IST, can be found in [26].

In this paper, we present several clarifications, extensions, and improvements in the application of the spin-domain Bloch equation inverse scattering transform as a tool for RF-pulse design. Before describing our results we briefly consider the older, Schrödinger approach. The idea is to reduce the Bloch equation to a scalar Schrödinger equation of the form

$$\partial_u^2 H + VH = 0. \tag{1}$$

Here $H(u)$ and $V(u)$ are complex valued functions. This reduction is accomplished by changes in both the dependent and independent variables. This approach led to several important advances, notably the so-called sech-pulses, see [23]. There are two basic reasons why it does not provide a good general framework for pulse design: (1) The change of variables, used to go from the

E-mail address: cle@math.upenn.edu.
[1] Research partially supported by NSF Grants DMS99-70487 and DMS02–07123.

1090-7807/$ - see front matter © 2004 Elsevier Inc. All rights reserved.
doi:10.1016/j.jmr.2003.12.014

Bloch equation to Eq. (1), is singular. (2) The inverse problem for the Schrödinger equation is not generally solvable for the sort of data that arise in RF-pulse synthesis. In particular this IST is poorly behaved if the potential, V, is complex valued. On the other hand, the transformation between the standard Bloch equation, and the spin-domain Bloch equation is smooth and invertible. The IST for the spin-domain equation is very well behaved for the data that arises in practical pulse synthesis problems. In this paper, we make no further mention of the Schrödinger approach to inverse scattering and pulse design.

The basic input to a pulse design problem is an ideal magnetization profile, $\boldsymbol{m}_i^\infty(v)$. This is a unit 3-vector-valued function of the offset frequency, v, which describes the state of the magnetization at the conclusion of the RF-pulse and possible rephasing. Typically, one would like to flip the spins through a specified angle, φ, for offset frequencies lying in a certain range $[v_0, v_1]$, and leave the spins in their equilibrium state for frequencies outside this interval. In principle, this is possible, and the pulse required to do it has finite energy. However, the instantaneous transition (in frequency space) would require an infinite amount of time to achieve. Hence, the first step in practical pulse design is the approximation of $\boldsymbol{m}_i^\infty(v)$ by a "design" magnetization profile, $\boldsymbol{m}_d^\infty(v)$, which can be (approximately) realized by a pulse of finite duration. In the SLR approach, $\boldsymbol{m}_i^\infty(v)$ is approximated by functions of a very specific form. This allows the construction of a pulse of a *given* duration. However, in return for fixing the duration of the pulse, one must give up directly specifying the phase of the transverse magnetization of $\boldsymbol{m}_d^\infty(v)$. Instead the phase is "recovered." In the IST approach one directly approximates $\boldsymbol{m}_i^\infty(v)$, but the duration of the pulse is not specified in advance. Strictly speaking, the pulses produced by the IST method have infinite duration. In practice this is not a problem, for if $\boldsymbol{m}_d^\infty(v)$ is reasonably smooth, then the pulse decays very rapidly. A short part of the pulse already produces a good approximation to $\boldsymbol{m}_d^\infty(v)$.

The design magnetization profile does *not* uniquely specify the pulse. Indeed, it is clear from inverse scattering theory that there is an *infinite dimensional* space of RF-envelopes that will produce any reasonable magnetization profile. The "auxiliary" data is specified by finite collections of pairs of complex numbers, $\{(\xi_1, C_1), \ldots, (\xi_N, C_N)\}$, with $\operatorname{Im}\xi_j > 0$ and $C_j \neq 0$. These are referred to as *bound states*. For any choice of $N \geqslant 0$, and bound states, there is a unique RF-envelope that produces the magnetization profile $\boldsymbol{m}_d^\infty(v)$. The remaining problem of pulse synthesis is therefore to choose bound states to obtain an "optimal" RF-envelope, producing a given magnetization profile. In this paper, we show how to use the IST approach to design RF-envelopes that utilize the minimum possible energy. At the center of this discussion is a formula expressing the energy in the RF-envelope explicitly in terms of the magnetization profile and the bound states. Formulæ of this type were discovered, in the context of inverse scattering for the Korteweg de Vries equation, by Zakharov and Faddeev [27]. The formula we use appears in a 1974 paper of Zakharov and Manakov [28]. A related, though less explicit formula, appears in [14]. This formula does not include contributions from the bound states. The formula we give is useful both for the design of pulse sequences, as well as for their analysis, as it allows for an a posteriori determination of the energy efficiency of a preexisting pulse sequence. It corrects the often repeated error in the MR-literature that the energy of a selective pulse is proportional to the square of the flip angle. In fact, the minimum energy required to flip spins in a band of width B, through an angle φ is proportional to $B\log(2/1+\cos\varphi)$. After this paper was completed it was brought to our attention that the formula for the energy appears in a paper of Rourke and Saunders [18].

Energy is just one among several important characteristics of a selective RF-pulse. Duration, maximum amplitude, stability, and rephasing time are also important parameters. While the minimum energy pulse may not be the best pulse for every application, it represents a good starting point when attempting to find that "best pulse." The other pulses producing a given magnetization profile have bound states. We give an extension of an algorithm, presented in [17], which allows for the specification of an essentially arbitrary collection of bound states. The formula for the energy shows that, for a given magnetization profile, a potential with bound states always requires more energy. It also is known, from the work of Morris and Rourke that, by adding bound states one can obtain truly self refocused pulses. But generally, the effects of bound states on the RF-envelope remain quite mysterious. Two very tantalizing questions are: (1) Can the duration of a pulse be reduced by adding bound states? See [7]. Can the sensitivity of a pulse to amplitude, or phase errors be reduced by adding bound states? Beyond these specific questions, it is clear that a large part of the flexibility in the design of RF-pulses resides in the selection of the bound states. Our algorithm opens up the possibility of systematically exploring their effects.

We close this introduction with a brief summary of the sections which follow. In Section 2 we recall the connection between the Bloch equation without relaxation, and its spin-domain formulation. Following the mathematics literature, we call this the *ZS-system*. We next review the scattering theory for the ZS-system, and relate the scattering data to the magnetization profile. These sections closely follow [1,14,17]. In Section 4 we state the formula relating the energy in the RF-envelope to the magnetization profile, and the location of the

bound states. In Section 5 we outline the inverse scattering transform for the ZS-equation. We use the Gel'fand–Levitan–Marchenko equation, or more briefly the Marchenko equation, following the treatment in [1]. In order to fix notation, and to have a complete and consistent foundation for further work in this field, these sections review some well known facts. In the Sections 6 and 7 we discuss the problem of implementing the IST, and give an algorithm for solving the Marchenko equation, with arbitrarily selected bound states. In Section 8 we compare the SLR and IST approaches. Section 9 contains a variety of examples. Proofs of several mathematical results are contained in an Appendix A.

2. The spin-domain Bloch equation and the problem of RF-pulse synthesis

The Bloch equation without relaxation is usually written in the form

$$\frac{\mathrm{d}\boldsymbol{M}}{\mathrm{d}t} = \gamma \boldsymbol{M} \times \boldsymbol{B}. \tag{2}$$

Here $\boldsymbol{M}$ is the magnetization, $\boldsymbol{B}$ is the applied magnetic field, t is time and γ is the gyromagnetic ratio. A vector evolves with constant length under this equation. Initial data is usually specified at $t = 0$; the solution to the Bloch equation is linear in the initial data. Throughout this paper we assume that solutions of the Bloch equation are normalized to have length equal to one.

The Bloch equation is usually analyzed in a "rotating reference" frame. Ordinarily the rotating reference frame is related to the "laboratory frame" by a time dependent orthogonal transformation of the form

$$\boldsymbol{F}(t) = \begin{bmatrix} \cos\theta(t) & -\sin\theta(t) & 0 \\ \sin\theta(t) & \cos\theta(t) & 0 \\ 0 & 0 & 1 \end{bmatrix}, \tag{3}$$

so that

$$\boldsymbol{M}(t) = \boldsymbol{F}(t)\boldsymbol{m}(t). \tag{4}$$

We use $\boldsymbol{m}$ to denote the magnetization in the rotating reference frame. Larmor's theorem implies that if $\boldsymbol{M}$ satisfies (2) then $\boldsymbol{m}$ satisfies

$$\frac{\mathrm{d}\boldsymbol{m}}{\mathrm{d}t} = \gamma \boldsymbol{m} \times \boldsymbol{B}_{\mathrm{eff}}, \tag{5}$$

where

$$\boldsymbol{B}_{\mathrm{eff}}(t) = \boldsymbol{F}^{-1}(t)\boldsymbol{B}(t) + \frac{1}{\gamma}\boldsymbol{\Omega}(t) \quad \text{with } \boldsymbol{\Omega}(t) = [0, 0, \theta'(t)]^{\dagger}. \tag{6}$$

Notational remark: Most of the vectors used in this paper are to be thought of a column vectors. The notation $[a, b, c]^{\dagger}$ refers to the transpose of the row vector, which is therefore a column vector, i.e.

$$[a, b, c]^{\dagger} = \begin{bmatrix} a \\ b \\ c \end{bmatrix}. \tag{7}$$

In most applications of this method, the function $\theta(t)$ is selected to render the z-component of $\boldsymbol{B}_{\mathrm{eff}}$ independent of time. Usually $\theta(t) = -\omega_0 t$, and

$$\boldsymbol{B}_{\mathrm{eff}}(v; t) = \left(\omega_1(t), \omega_2(t), \gamma^{-1}v\right). \tag{8}$$

The constant value v is called the *offset frequency* or *resonance offset*. If $\boldsymbol{B}_{\mathrm{eff}}$ is given by (8), then, in the laboratory frame, the RF-envelope is given by

$$\boldsymbol{B}_1(t) = \left[\mathrm{Re}\, \mathrm{e}^{\mathrm{i}\theta(t)}(\omega_1(t) + \mathrm{i}\omega_2(t)), \mathrm{Im}\, \mathrm{e}^{\mathrm{i}\theta(t)}(\omega_1(t) + \mathrm{i}\omega_2(t)), 0\right]^{\dagger}. \tag{9}$$

The energy in the RF-envelope is given by

$$E_p = \int_{-\infty}^{\infty} |\boldsymbol{B}_1(t)|^2 \,\mathrm{d}t = \int_{-\infty}^{\infty} |\omega_1(t) + \mathrm{i}\omega_2(t)|^2 \,\mathrm{d}t. \tag{10}$$

A magnetization profile is a unit vector valued function defined for $v \in \mathbb{R}$

$$\boldsymbol{m}^{\infty}(v) = \begin{bmatrix} m_1^{\infty}(v) \\ m_2^{\infty}(v) \\ m_3^{\infty}(v) \end{bmatrix}. \tag{11}$$

In essentially all MR applications, $\boldsymbol{m}^{\infty}(v) = [0, 0, 1]^{\dagger}$, for v outside of a bounded interval. The problem of RF-pulse synthesis is to find a time dependent complex pulse envelope, $\omega_1(t) + \mathrm{i}\omega_2(t)$, so that, if $\boldsymbol{B}_{\mathrm{eff}}(v)$ is given by (8), then the solution of

$$\frac{\mathrm{d}\boldsymbol{m}}{\mathrm{d}t}(v; t) = \gamma \boldsymbol{m}(v; t) \times \boldsymbol{B}_{\mathrm{eff}}(v; t), \tag{12}$$

with

$$\lim_{t \to -\infty} \boldsymbol{m}(v; t) = [0, 0, 1]^{\dagger}, \tag{13}$$

satisfies

$$\lim_{t \to \infty} \left[\mathrm{e}^{-\mathrm{i}vt}(m_1 + \mathrm{i}m_2)(v; t), m_3(v; t)\right] = \left[\left(m_1^{\infty} + \mathrm{i}m_2^{\infty}\right)(v), m_3^{\infty}(v)\right]. \tag{14}$$

We have used the standard complex notation, $m_1 + \mathrm{i}m_2$, for the transverse components of the magnetization. If $\omega_1(t) + \mathrm{i}\omega_2(t)$ is supported in the interval $[t_0, t_1]$, then these asymptotic conditions are replaced by

$$\boldsymbol{m}(v; t_0) = [0, 0, 1]^{\dagger}, \quad \left[\mathrm{e}^{-\mathrm{i}vt_1}(m_1 + \mathrm{i}m_2)(v; t_1), m_3(v; t_1)\right] = \left[\left(m_1^{\infty} + \mathrm{i}m_2^{\infty}\right)(v), m_3^{\infty}(v)\right]. \tag{15}$$

The mapping from $\omega_1(t) + \mathrm{i}\omega_2(t)$ to $\boldsymbol{m}^{\infty}$ (as defined in Eqs. (12)–(14)) is highly nonlinear; the problem of pulse synthesis is that of inverting this mapping.

To solve the problem of RF-pulse synthesis, it is convenient to introduce the spin domain formulation of the Bloch equation. Instead of a unit vector $\boldsymbol{m}$ in $\mathbb{R}^3$, we

solve for a unit vector $\boldsymbol{\psi}$ in $\mathbb{C}^2$. This vector satisfies the 2×2 matrix equation

$$\frac{\mathrm{d}\boldsymbol{\psi}}{\mathrm{d}t} = -\frac{\mathrm{i}}{2}\,\boldsymbol{\omega}\cdot\boldsymbol{\sigma}\boldsymbol{\psi}. \tag{16}$$

Here $\boldsymbol{\omega} = -[\gamma\omega_1(t), \gamma\omega_2(t), v]$, and $\boldsymbol{\sigma}$ are the Pauli spin matrices:

$$\sigma_1 = \begin{bmatrix} 0 & 1 \\ 1 & 0 \end{bmatrix}, \quad \sigma_2 = \begin{bmatrix} 0 & -\mathrm{i} \\ \mathrm{i} & 0 \end{bmatrix}, \quad \sigma_3 = \begin{bmatrix} 1 & 0 \\ 0 & -1 \end{bmatrix}. \tag{17}$$

Assembling the pieces we see that $\boldsymbol{\psi}$ satisfies[2]

$$\frac{\mathrm{d}\boldsymbol{\psi}}{\mathrm{d}t}(\xi;t) = \begin{bmatrix} -\mathrm{i}\xi & q(t) \\ -q^*(t) & \mathrm{i}\xi \end{bmatrix}\boldsymbol{\psi}(\xi;t), \tag{18}$$

with

$$\xi = \frac{v}{2}, \quad q(t) = \frac{-\mathrm{i}\gamma}{2}(\omega_1(t) - \mathrm{i}\omega_2(t)). \tag{19}$$

A simple recipe takes a solution of (18) and produces a solution of (12). If $\boldsymbol{\psi}(\xi;t) = [\psi_1(\xi;t), \psi_2(\xi;t)]^\dagger$ satisfies (18) then the 3-vector

$$\boldsymbol{m}(v;t) = \Big[2\,\mathrm{Re}\,(\psi_1^*\psi_2), 2\,\mathrm{Im}\,(\psi_1^*\psi_2), |\psi_1|^2 - |\psi_2|^2\Big]^\dagger\Big(\frac{v}{2};t\Big), \tag{20}$$

satisfies (12). If in addition

$$\lim_{t\to-\infty} \mathrm{e}^{\mathrm{i}\xi t}\boldsymbol{\psi}(\xi;t) = \begin{bmatrix} 1 \\ 0 \end{bmatrix}, \tag{21}$$

then $\boldsymbol{m}$ satisfies (13). Thus the RF-pulse synthesis problem is easily translated into a inverse scattering problem for Eq. (18). This is described in the next section. Following the standard practice in inverse scattering we refer to Eq. (18) as the *ZS-system* and q as the *potential*. Our presentation of the spin domain Bloch equation is largely taken from [17]. The only difference in our normalization is that we have not rescaled the time variable; for comparisons, set $T = 1$ in [17].

3. Scattering theory for the ZS-system

Scattering theory for an equation like (18) relates the behavior of $\boldsymbol{\psi}(\xi;t)$, as $t\to-\infty$ to that of $\boldsymbol{\psi}(\xi;t)$, as $t\to+\infty$. If q has bounded support, then the functions

$$\begin{bmatrix} \mathrm{e}^{-\mathrm{i}\xi t} \\ 0 \end{bmatrix}, \quad \begin{bmatrix} 0 \\ \mathrm{e}^{\mathrm{i}\xi t} \end{bmatrix}, \tag{22}$$

are a basis of solutions for (18) outside the support of q. If the L^1-norm of q is finite, then, it is shown in [1], that (18) has solutions that are asymptotic to these solutions as $t\to\pm\infty$.

[2] We follow the standard practice in the MR literature of using z^* to denote the complex conjugate of the complex number z.

Theorem 1. *If $\|q\|_{L^1}$ is finite, then, for every real ξ, there are* unique *solutions*

$$\boldsymbol{\psi}_{1+}(\xi), \boldsymbol{\psi}_{2+}(\xi) \text{ and } \boldsymbol{\psi}_{1-}(\xi), \boldsymbol{\psi}_{2-}(\xi), \tag{23}$$

to Eq. (18), *which satisfy*:

$$\lim_{t\to-\infty} \mathrm{e}^{\mathrm{i}\xi t}\boldsymbol{\psi}_{1-}(\xi;t) = \begin{bmatrix} 1 \\ 0 \end{bmatrix}, \quad \lim_{t\to-\infty} \mathrm{e}^{-\mathrm{i}\xi t}\boldsymbol{\psi}_{2-}(\xi;t) = \begin{bmatrix} 0 \\ -1 \end{bmatrix}, \tag{24}$$

$$\lim_{t\to\infty} \mathrm{e}^{\mathrm{i}\xi t}\boldsymbol{\psi}_{1+}(\xi;t) = \begin{bmatrix} 1 \\ 0 \end{bmatrix}, \quad \lim_{t\to\infty} \mathrm{e}^{-\mathrm{i}\xi t}\boldsymbol{\psi}_{2+}(\xi;t) = \begin{bmatrix} 0 \\ 1 \end{bmatrix}. \tag{25}$$

The solutions $\boldsymbol{\psi}_{1-}(\xi), \boldsymbol{\psi}_{2+}(\xi)$ extend as analytic functions of ξ to the upper half plane, $\{\xi : \mathrm{Im}\,\xi > 0\}$, and $\boldsymbol{\psi}_{2-}(\xi), \boldsymbol{\psi}_{1+}(\xi)$ extend as analytic functions of ξ to the lower half plane, $\{\xi : \mathrm{Im}\,\xi < 0\}$.

The proof of this theorem can be found in [1].

For real values of ξ, the solutions normalized at $-\infty$ can be expressed in terms of the solutions normalized at $+\infty$ by linear relations:

$$\begin{aligned} \boldsymbol{\psi}_{1-}(\xi;t) &= a(\xi)\boldsymbol{\psi}_{1+}(\xi;t) + b(\xi)\boldsymbol{\psi}_{2+}(\xi;t), \\ \boldsymbol{\psi}_{2-}(\xi;t) &= b^*(\xi)\boldsymbol{\psi}_{1+}(\xi;t) - a^*(\xi)\boldsymbol{\psi}_{2+}(\xi;t). \end{aligned} \tag{26}$$

The functions a, b are called the *scattering coefficients* for the potential q. The 2×2-matrices $[\boldsymbol{\psi}_{1-}\boldsymbol{\psi}_{2-}], [\boldsymbol{\psi}_{1+}\boldsymbol{\psi}_{2+}]$ satisfy

$$[\boldsymbol{\psi}_{1-}\boldsymbol{\psi}_{2-}] = [\boldsymbol{\psi}_{1+}\boldsymbol{\psi}_{2+}]\begin{bmatrix} a(\xi) & b^*(\xi) \\ b(\xi) & -a^*(\xi) \end{bmatrix}. \tag{27}$$

The *scattering matrix* for the potential q is defined to be

$$s(\xi) = \begin{bmatrix} a(\xi) & b^*(\xi) \\ b(\xi) & -a^*(\xi) \end{bmatrix}. \tag{28}$$

Recall that the *Wronskian* between two $\mathbb{C}^2$-valued functions of t is defined by

$$W(\boldsymbol{u}(t), v(t)) \stackrel{d}{=} u_1(t)v_2(t) - u_2(t)v_1(t). \tag{29}$$

If $\boldsymbol{u}(t)$ and $\boldsymbol{v}(t)$ are solutions of (18), for the same value of ξ, then $W(\boldsymbol{u}(t), \boldsymbol{v}(t))$ is independent of t. In this case we denote the Wronskian by $W(\boldsymbol{u}, \boldsymbol{v})$. It is not difficult to show that

$$\begin{aligned} a(\xi) &= [\psi_{11-}(\xi;t)\psi_{22+}(\xi;t) - \psi_{21-}(\xi;t)\psi_{12+}(\xi;t)] \\ &= W(\boldsymbol{\psi}_{1-}, \boldsymbol{\psi}_{2+})(\xi). \end{aligned} \tag{30}$$

It follows from Theorem 1 and (30) that a extends to the upper half plane as an analytic function.

If q has an integrable derivative, then (30) implies that

$$a(\xi) = 1 + \frac{1}{2\mathrm{i}\xi}\int_{-\infty}^{\infty} |q(s)|^2\,\mathrm{d}s + \mathrm{O}\Big(\frac{1}{\xi^2}\Big), \tag{31}$$

as $|\xi|$ tends to infinity in $\mathrm{Im}\,\xi \geqslant 0$. As $W(\boldsymbol{\psi}_{1-}, \boldsymbol{\psi}_{2-}) = -1$ it follows that:

$$|a(\xi)|^2 + |b(\xi)|^2 = 1, \tag{32}$$

and therefore (31) implies that

$$|b(\xi)| = \mathrm{O}\left(\frac{1}{|\xi|}\right) \quad \text{as } \xi \to \pm\infty. \tag{33}$$

These results are proved in [1].

Assuming that $t^j q(t)$ is integrable for all j it is shown in [1] that a has finitely many zeros in $\mathrm{Im}\,\xi \geqslant 0$. The Wronskian, $W(\boldsymbol{\psi}_{1-}, \boldsymbol{\psi}_{2+})(\xi)$ vanishes if and only if the functions $\boldsymbol{\psi}_{1-}$ and $\boldsymbol{\psi}_{2+}$ are linearly dependent. Let $\{\xi_1, \ldots, \xi_N\}$ be a list of the zeros of a. Formula (30) implies that for each j there is a *nonzero* complex number C_j' so that

$$\boldsymbol{\psi}_{1-}(\xi_j) = C_j' \boldsymbol{\psi}_{2+}(\xi_j), \quad j = 1, \ldots, N. \tag{34}$$

Eq. (18) can be rewritten in the form

$$\begin{bmatrix} \mathrm{i}\partial_t & -\mathrm{i}q \\ -\mathrm{i}q^* & -\mathrm{i}\partial_t \end{bmatrix} \begin{bmatrix} \psi_1 \\ \psi_2 \end{bmatrix} = \xi \begin{bmatrix} \psi_1 \\ \psi_2 \end{bmatrix}. \tag{35}$$

From this formulation it is clear that ξ should be regarded as a spectral parameter. If ξ has positive imaginary part, then $\boldsymbol{\psi}_{1-}(\xi; t)$ decays exponentially as t tends to $-\infty$ and $\boldsymbol{\psi}_{2+}(\xi; t)$ decays exponentially as t tends to $+\infty$. Hence (34) implies that $\boldsymbol{\psi}_{1-}(\xi_j; t)$ decays exponentially at both $\pm\infty$ and therefore the function $\boldsymbol{\psi}_{1-}(\xi_j; t)$ belongs to $L^2(\mathbb{R}; \mathbb{C}^2)$. Thus the operator on the left-hand side of (35) has L^2-*bound states* for these values of the offset frequency.

We generally assume that the zeros of a are simple and that their imaginary parts are positive. This is mostly to simplify the exposition, there is no difficulty, in principle, if a has real zeros or higher order zeros.

Definition 1. The pair of functions $(a(\xi), b(\xi))$, for $\xi \in \mathbb{R}$, and the collection of pairs $\{(\xi_j, C_j') : j = 1, \ldots, N\}$ define the *scattering data* for Eq. (18).

The scattering data are not independent. If $\{\xi_j : j = 1, \ldots, N\}$ are the zeros of $a(\xi)$ in the upper half plane, then

$$\tilde{a}(\xi) = \prod_{j=1}^{N} \left(\frac{\xi - \xi_j^*}{\xi - \xi_j}\right) a(\xi), \tag{36}$$

is an analytic function without zeros in the upper half plane. Moreover $|a(\xi)| = |\tilde{a}(\xi)|$ on the real axis. The function $\log \tilde{a}$ is also analytic in the upper half plane, and the asymptotic formula (31) implies that $|\log \tilde{a}(\xi)|$ is $\mathrm{O}(|\xi|^{-1})$ as $|\xi|$ tends to infinity. The Cauchy integral formula therefore applies to give a representation of $\log \tilde{a}$ in $\mathrm{Im}\,\xi > 0$

$$\log \tilde{a}(\xi) = \frac{1}{2\pi\mathrm{i}} \int_{-\infty}^{\infty} \frac{\log(|a(\zeta)|^2)\,\mathrm{d}\zeta}{\zeta - \xi}. \tag{37}$$

Exponentiating, and putting the zeros of a back in gives

$$a(\xi) = \prod_{j=1}^{N} \left(\frac{\xi - \xi_j}{\xi - \xi_j^*}\right) \exp\left[\frac{1}{2\pi\mathrm{i}} \int_{-\infty}^{\infty} \frac{\log(|a(\zeta)|^2)\,\mathrm{d}\zeta}{\zeta - \xi}\right], \tag{38}$$

see [6]. The *reflection* coefficient is defined by

$$r(\xi) = \frac{b(\xi)}{a(\xi)}. \tag{39}$$

A priori the reflection coefficient is only defined on the real axis. Using (32) we rewrite (38) in terms of r

$$a(\xi) = \prod_{j=1}^{n} \left(\frac{\xi - \xi_j}{\xi - \xi_j^*}\right) \exp\left[\frac{\mathrm{i}}{2\pi} \int_{-\infty}^{\infty} \frac{\log(1 + |r(\zeta)|^2)\,\mathrm{d}\zeta}{\zeta - \xi}\right]. \tag{40}$$

Both (38) and (40) have well defined limits as ξ approaches the real axis.

If a has simple zeros at the points $\{\xi_1, \ldots, \xi_N\}$ (so that $a'(\xi_j) \neq 0$), then we define the *norming constants* by setting

$$C_j = \frac{C_j'}{a'(\xi_j)}, \tag{41}$$

where the $\{C_j'\}$ are defined in (34). The definition needs to be modified if a has nonsimple zeros. The reason for replacing $\{C_j'\}$ with $\{C_j\}$ will become more apparent in Section 5. The pairs $\{(\xi_j, C_j)\}$ are often referred to as the *discrete data*.

Definition 2. The function $r(\xi)$, for $\xi \in \mathbb{R}$, and the collection of pairs $\{(\xi_j, C_j) : j = 1, \ldots, N\}$ define the *reduced scattering data* for Eq. (18).

Implicitly the reduced scattering data is a function of the potential q. In inverse scattering theory, the data $\{r(\xi) \text{ for } \xi \in \mathbb{R}; (\xi_{\mathbb{1}}, C_1), \ldots, (\xi_{\mathbb{N}}, C_N)\}$ are specified, and we seek a potential q that has this reduced scattering data. The map from the reduced scattering data to q is often called the *Inverse Scattering Transform* or *IST*.

Remark 1. In some of the mathematical and MR literature there is confusion about the relationship between possible poles of r in the upper half plane and the locations of bound states. It is important to realize that a priori there is *no* connection between poles of r in the upper half plane and the bound states. This is illustrated in example 3.

We now rephrase the RF-pulse synthesis problem as an inverse scattering problem. Recall that the data for the pulse synthesis problem is the magnetization profile $\boldsymbol{m}^\infty$, which we now think of as a function of $\xi = v/2$. Using (20), the solution $\boldsymbol{\psi}_{1-}$ to the ZS-system defines a solution $\boldsymbol{m}_{1-}$ to (12), satisfying (13). It follows from (25) and (26) that

$$\boldsymbol{\psi}_{1-}(\xi;t) \sim \begin{bmatrix} a(\xi)\mathrm{e}^{-\mathrm{i}\xi t} \\ b(\xi)\mathrm{e}^{\mathrm{i}\xi t} \end{bmatrix}, \quad \text{as } t \to +\infty. \tag{42}$$

Therefore

$$\boldsymbol{m}_{1-}(\xi;t) \sim \begin{bmatrix} 2b(\xi)a^*(\xi)\mathrm{e}^{2\mathrm{i}\xi t} \\ |a(\xi)|^2 - |b(\xi)|^2 \end{bmatrix}, \quad \text{as } t \to +\infty. \tag{43}$$

As before, we use the complex notation for the transverse components of $\boldsymbol{m}_{1-}$. If $\boldsymbol{m}_{1-}$ also satisfies (14), then it follows from (43) and (32) that:

$$\begin{aligned} r(\xi) &= \frac{b(\xi)}{a(\xi)} = \lim_{t\to\infty} \frac{(m_{11-} + \mathrm{i}m_{21-})(\xi;t)\mathrm{e}^{-2\mathrm{i}\xi t}}{1 + m_{31-}(\xi;t)} \\ &= \frac{(m_1^\infty + \mathrm{i}m_2^\infty)(\xi)}{1 + m_3^\infty(\xi)}. \end{aligned} \tag{44}$$

If q has support in the ray $(-\infty, t_1]$ then

$$r(\xi) = \frac{(m_{11-} + \mathrm{i}m_{21-})(\xi;t)\mathrm{e}^{-2\mathrm{i}\xi t}}{1 + m_{31-}(\xi;t)}, \tag{45}$$

is independent of t for $t \geqslant t_1$. It is also useful to observe that if $r(\xi)$ is the reflection coefficient, determined by the potential $q(t)$, then $\mathrm{e}^{-2\mathrm{i}\tau\xi}r(\xi)$ is the reflection coefficient determined by the time shifted potential $q_\tau(t) = q(t-\tau)$.

As $\boldsymbol{m}^\infty(\xi)$ is a unit vector valued function, we see that the reflection coefficient $r(\xi)$ uniquely determines $\boldsymbol{m}^\infty(\xi)$ and vice-versa. Thus the RF-pulse synthesis problem can be rephrased as the following inverse scattering problem: Find a potential $q(t)$ for the ZS-system so that the reflection coefficient $r(\xi)$ satisfies (44) for all real ξ. Note that the pulse synthesis problem makes no reference to the data connected with the bound states, i.e., $\{(\xi_j, C_j)\}$. Indeed these are *free* parameters in the RF-pulse synthesis problem, making the problem highly underdetermined. A basic result of this paper is that, for a given magnetization profile, the RF-envelope requiring the minimum energy is the one for which the ZS-system has *no* bound states.

Remark 2. It is useful to consider the physical significance of the t-parameter that appears in (16), and its connection to the problem of rephasing. The main clue comes from (45). Suppose that $q(t)$ is a potential supported in $[t_0, t_1]$ with reflection coefficient r. After time t_1, a solution to (16) is freely precessing in the local (gradient offset) $\boldsymbol{B}_0$-field. If $t_1 = 0$, then, at the end of the RF-excitation, the magnetization satisfies

$$\frac{(m_{11-} + \mathrm{i}m_{21-})(\xi;0)}{1 + m_{31-}(\xi;0)} = r(\xi). \tag{46}$$

We have therefore achieved the desired magnetization profile, without any need for rephasing. Pulses supported in $(-\infty, 0]$ are therefore self refocused. If on the other hand $t_1 < 0$, then, at the end of the excitation, the magnetization satisfies

$$\frac{(m_{11-} + \mathrm{i}m_{21-})(\xi;t_1)}{1 + m_{31-}(\xi;t_1)} = \mathrm{e}^{2\mathrm{i}\xi t_1}r(\xi). \tag{47}$$

In order to get the desired magnetization profile, the spins must freely precess for $|t_1|$-units of time. Finally if $t_1 > 0$ (as it normally is), then the spins must precess for $-t_1$-units of time. In order to achieve the magnetization profile *specified by* r, either a 180°-refocusing pulse must be applied, or the gradient needs to be reversed, followed by t_1-units of free precession. For pulses designed using the magnetization profile itself, it is natural to call t_1 the rephasing time. However, in many instances, e.g., in SLR, pulses are *not* designed using the magnetization profile, (or reflection coefficient), but rather, by using the flip angle.

The *flip angle profile*, $\varphi(\xi)$, is related to the scattering data by

$$\varphi(\xi) = \sin^{-1}\left(\frac{2|r(\xi)|}{1 + |r(\xi)|^2}\right) = 2\sin^{-1}(|b(\xi)|). \tag{48}$$

SLR pulses are usually designed using the flip angle profile and, the phase of the reflection coefficient is determined indirectly. It is said that the phase is "recovered." In this context the reflection coefficient determined by the pulse envelope is an approximation to a function of the form $\mathrm{e}^{\mathrm{i}\phi(\xi)}r(\xi)$, where $r(\xi)$ is the "ideal" reflection coefficient. If $\phi(\xi)$ is approximately linear over the support of $r(\xi)$, then the magnetization can be approximately rephased. In this case, the actual rephasing time comes in part from t_1, as before, and in part from the phase factor, $\mathrm{e}^{\mathrm{i}\phi(\xi)}$. We return to this point in our discussion of SLR pulse design in Section 8.

Another context where the phase of $r(\xi)$ is not specified in advance is in "minimum phase" pulse design. To illustrate this point we consider the example of a 90°, "minimum phase," minimum energy IST pulse. For this pulse, $r_s(\xi)$ is a smooth approximation to the characteristic function of an interval. The pulse is designed using a reflection coefficient of the form

$$r_d(\xi) = r_s(\xi)\prod_{j=1}^{N}\left(\frac{\xi - \xi_j}{\xi - \xi_j^*}\right). \tag{49}$$

The Blaschke product in (49) has modulus one on the real axis. The complex numbers $\{\xi_j\}$ are selected so that the resultant pulse has support in $(-\infty, 0]$. Fig. 1A shows the pulse, which is, in fact, supported in $(-\infty, 0]$. Fig. 1B shows the transverse magnetization corresponding to the reflection coefficient, $r_d(\xi)$, used to design the pulse. Fig. 1C shows the transverse magnetization attainable by using 4.93 ms of additional rephasing time. The minimum energy pulse, with the same absolute magnetization profile, has approximately the same duration as the minimum phase pulse, but requires about 15 ms to rephase. A truly self refocused 90° pulse has about the same duration, as the

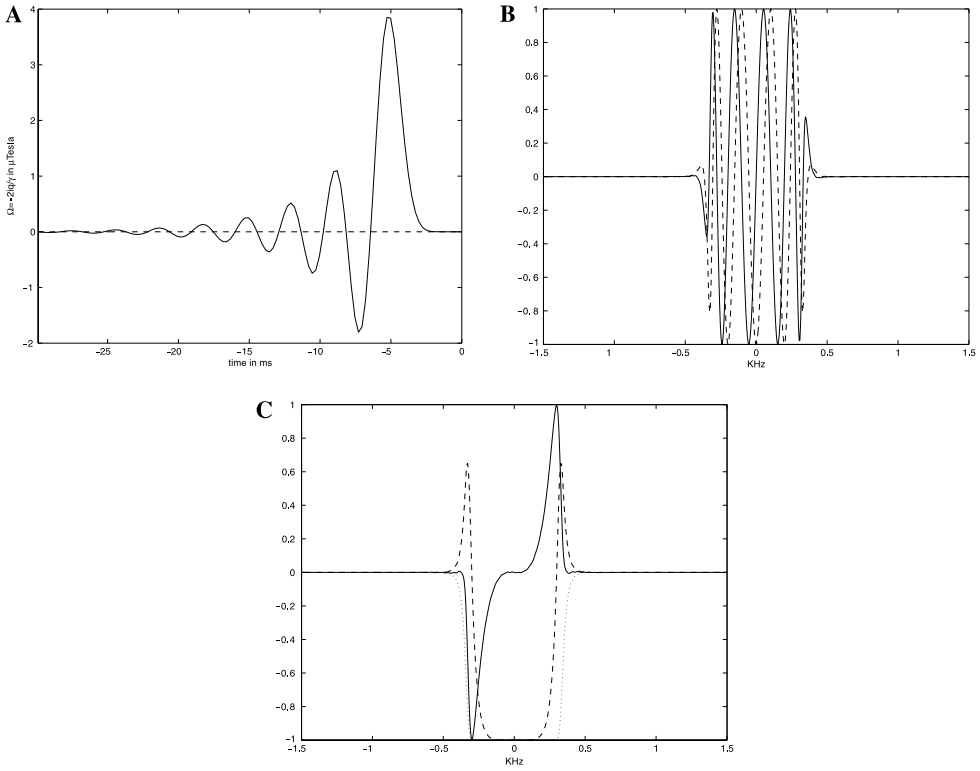

Fig. 1. This is an example of a minimum phase (IST) pulse, designed using the flip angle profile, without direct control on the phase of the magnetization. It illustrates how a reasonably good magnetization profile can still be attained by using additional rephasing time, over and above what is predicted by the upper limit of the support of the potential. (A) A 90° minimum phase pulse. (B) The transverse magnetization given by the reflection coefficient used to design the pulse in (A). (Solid line $= m_1$, dashed line $= m_2$.) (C) The magnetization profile attainable by rephasing the profile shown in (B) for an additional 4.93 ms. For comparison $-|m_{xy}|$ is shown as a dotted line.

minimum phase-minimum energy pulse. But has both much larger energy and maximum amplitude. It produces a much cleaner magnetization profile. See $q_3^+(t)$ in Example 4.

Remark 3. In RF-pulse synthesis, the data is specified in the *frequency* domain. Given $r(\xi)$, and perhaps some bound states $\{(\xi_j, C_j)\}$, the IST produces a potential, which is a function of t. The time parameterization of this potential is determined by the reduced scattering data and thereby determines what sort of rephasing is needed to achieve the specified magnetization profile. In the IST approach the reflection coefficient is usually taken to have bounded support. The Paley–Wiener theorem for inverse scattering, see [22], implies that the corresponding potential, $q(t)$, therefore cannot have bounded support.

For practical applications one therefore needs to select a finite part of $q(t)$. In this context we speak of the *effective* support of the potential. Operationally, an interval $[t_0, t_1]$ contains the effective support of $q(t)$ if, for some window function, $w(t)$, supported in $[t_0, t_1]$, the reflection coefficient, $r_w(\xi)$, of the windowed potential, $w(t)q(t)$, is a sufficiently good approximation to $r(\xi)$, over a given interval. So long as there are no bound states, the support properties of $q(t)$ are largely determined by the smoothness of $r(\xi)$. If $r(\xi)$ has a very sharp transition, then $q(t)$ dies off very slowly. In order to achieve a good approximation to $r(\xi)$, a long part of $q(t)$ is required. On the other hand, if $r(\xi)$ has only smooth (i.e., long) transitions, then $q(t)$ dies off very quickly. In principle, there is no difficulty in attaining an arbitrarily sharp transition in the magnetization profile. In practice the required pulse is so long that relaxation effects will dominate. Fig. 2A shows a minimum energy IST pulse, truncated to show all values where the pulse assumes at least 0.01% of its maximum amplitude, this part of the pulse is 200 ms long. Fig. 2B shows the transverse magnetization profile it produces. The width of the transition region, on each side, is about 5% of the width of the passband.

The choice of window function is an important topic in the practical application of IST pulses. Generally speaking, cutting off a potential has the effect of reducing its selectivity and introducing phase errors. For minimum energy pulses, the magnetization profile changes gradually as the support of a smooth window function is decreased. A sharp cutoff can lead $r_w(\xi)$ to display considerable oscillations. A potential with bound states often has a large maximum amplitude. In

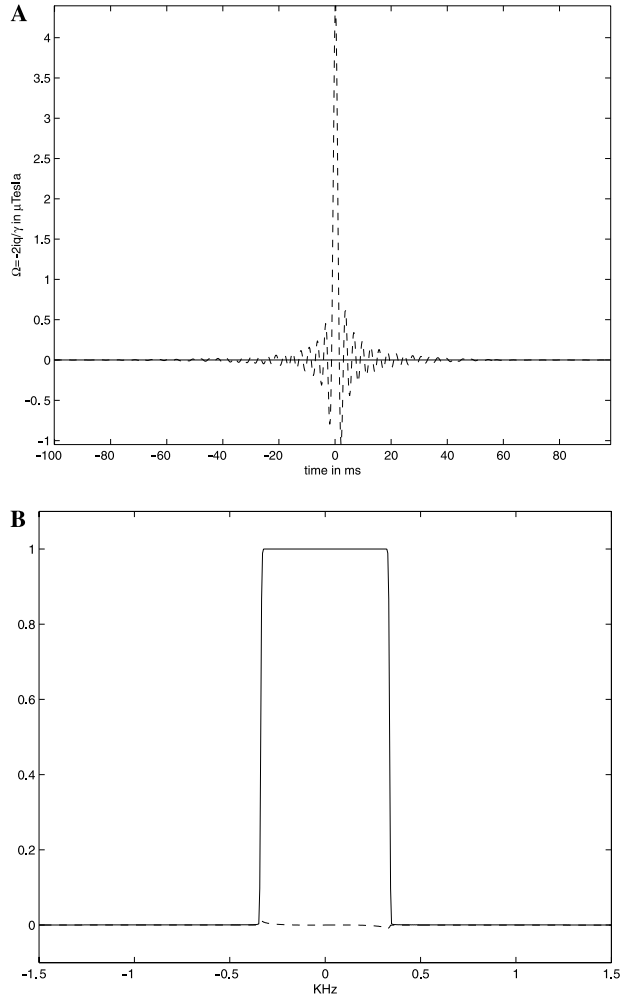

Fig. 2. A minimum energy 90° IST pulse, which produces a very sharp transition. The pulse duration is about 200 ms and the bandwidth of the excitation is about 700 Hz. (A) A 90° minimum energy IST pulse with a very sharp transition region. (B) The transverse magnetization produced by the pulse in (A). (Solid line = m_1, dashed line = m_2.)

examples, we have observed that parts of these potentials with small *relative* amplitude are quite important for achieving the desired magnetization profile. Hence, if there are bound states, the problem of windowing becomes rather subtle. We therefore leave a careful analysis of this question to a future publication. For the moment we consider only a simple, minimum energy example.

Fig. 3 shows three truncations of a minimum energy 90° IST pulse, along with the magnetization profiles they produce. Fig. 3A shows the pulse sharply truncated to an interval containing all points, where it assumes at least 0.001% of its maximum amplitude. Fig. 3C shows the pulse, again truncated sharply, to the interval where it assumes at least 1% of its maximum amplitude. Finally in Fig. 3E we show the segment of the pulse shown in Fig. 3C but windowed by a function vanishing near the end points of the interval. The corresponding magnetization profiles are shown in Figs. 3B, D, and F. Using the 0.001% criterion gives a pulse of finite duration producing (within the displayed interval) an almost perfect magnetization profile. Because, in Fig. 3C, $q(t)$ is fairly large near the points where it is being truncated, the sharp truncation produces the oscillations seen in Fig. 3D. Smoothing this transition removes the large oscillations, but leads to the larger, localized phase errors seen in Fig. 3F.

Remark 4. Our discussion of inverse scattering and its applications to RF-pulse design is largely adapted from [1,14,17].

4. The energy of the RF-envelope

We now state a formula for the energy of the pulse envelope in terms of the reduced scattering data. The underlying results from inverse scattering theory are due to Zakharov, Faddeev, and Manakov. This formula is related to formula (19) in [14]. Using this formula one can approximately determine the energy in an SLR-pulse in terms of a parameter, a_0, arising in the SLR method. Using a contour integral argument, one can deduce an expression for a_0 in terms of the bound states, and reflection coefficient, and thereby obtain a formula quite similar to Eq. (50) below. To the best of my knowledge, no such formula appears in the MR-literature.[3]

Theorem 2. *Suppose that $q(t)$ is a sufficiently rapidly decaying potential for the ZS-system, with reflection coefficient $r(\xi)$, and discrete data $\{(\xi_j, C_j), j = 1, \ldots, N\}$, then*

$$\int_{-\infty}^{\infty} |q(t)|^2 \, \mathrm{d}t = \frac{1}{\pi} \int_{-\infty}^{\infty} \log(1 + |r(\xi)|^2) \, \mathrm{d}\xi + 4 \sum_{j=1}^{N} \operatorname{Im} \xi_j. \tag{50}$$

The proof of this result can be found in [1] or [6]. Note that the norming constants play no role in this formula. Formula (50) is just one from an infinite sequence of formulæ relating functionals of the potential to functionals of the reduced scattering data, see [6].

Combining Eqs. (10), and (50) with (44) we obtain the following simple corollary.

[3] After this paper was completed it was brought to our attention that formula (50), along with the conclusion that the minimum energy pulse is the one with no bound states, appears in a paper of Rourke and Saunders [18].

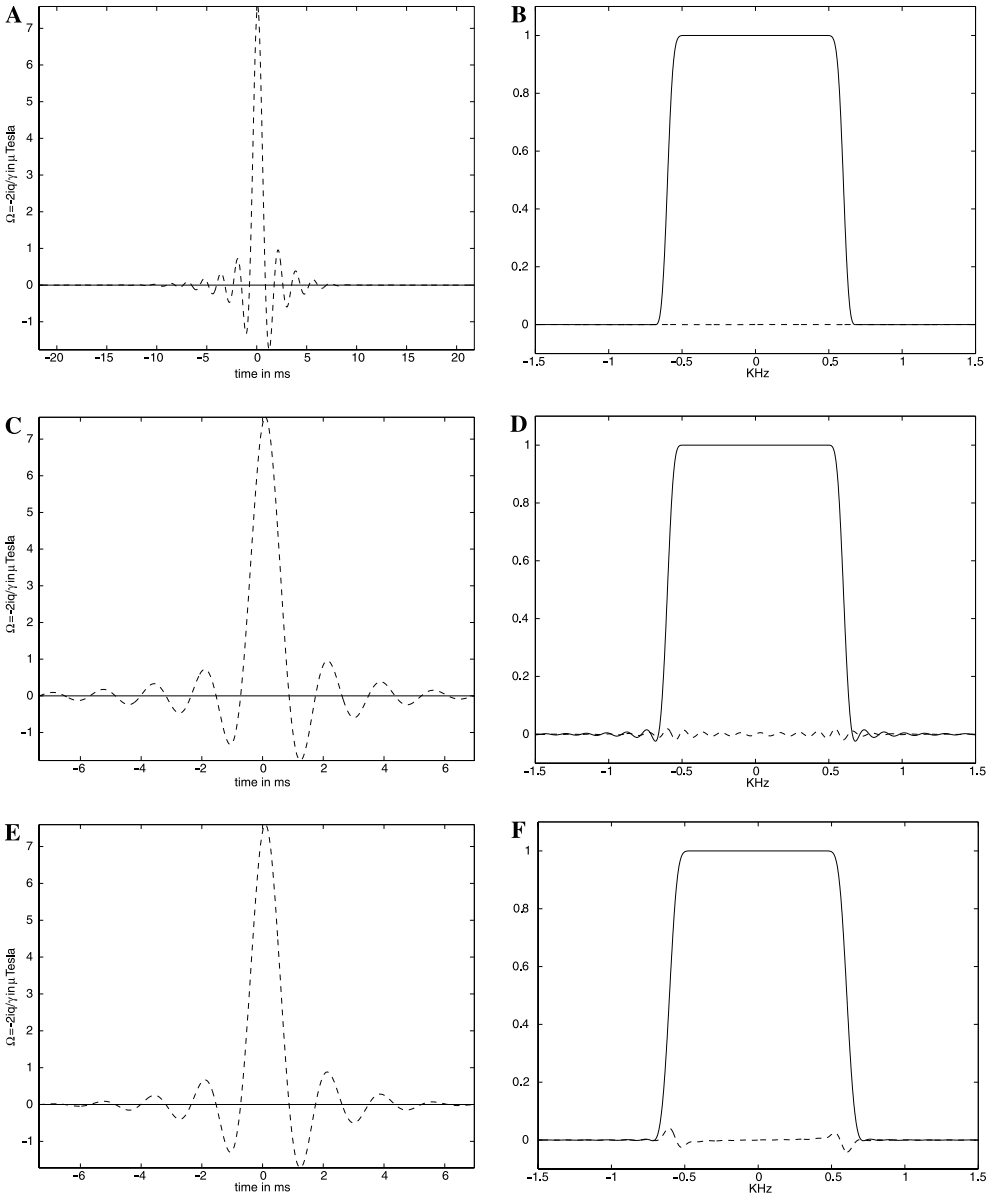

Fig. 3. Various truncations of a 90°, minimum energy, IST pulse, and the magnetization profiles they produced. (A) Sharp truncation by 0.0s% criterion. (B) Transverse magnetization produced by (A). (C) Sharp truncation by 1% criterion. (D) Transverse magnetization produced by (C). (E) Smooth truncation by 1% criterion. (F) Transverse magnetization produced by (E).

Corollary 1. *If* $\boldsymbol{m}^{\infty}$ *is a sufficiently smooth magnetization profile such that* $m_1^{\infty} + \mathrm{i}m_2^{\infty}$ *decays to zero as* $|\xi| \to \infty$, *and is square integrable, then the total energy of* any *RF-envelope,* $\omega_1(t) + \mathrm{i}\omega_2(t)$, *which produces this magnetization profile, satisfies the estimate*

$$\int_{-\infty}^{\infty} |\omega_1(t) + \mathrm{i}\omega_2(t)|^2 \,\mathrm{d}t \geqslant \frac{2}{\pi\gamma^2} \int_{-\infty}^{\infty} \log\left(1 + \left|\frac{m_1^{\infty}(\xi) + \mathrm{i}m_2^{\infty}(\xi)}{1 + m_3^{\infty}(\xi)}\right|^2\right) \mathrm{d}\xi. \quad (51)$$

Equality holds in this estimate if and only if the ZS-system with the corresponding potential has no bound states.

Note that the energy depends only on the flip angle, and not on the phase of the magnetization profile. Indeed, the argument of the log in (51) can be rewritten as $2(1 + m_3(\xi))^{-1}$. From the corollary it is evident that the lowest energy RF-envelope is obtained by solving the inverse scattering problem with *no* bound states.

Example 1. A common way to construct a selective 90°-pulse is to approximate $r(\xi)$ by a function of the form $r_n(\xi) = (1 + \xi^{2n})^{-1}$. To obtain a minimum energy pulse, one can use, as the reduced scattering data, $r_n(\xi)$, for ξ on the real axis with no bound states. Using formula (50), we see that the energy of the minimum energy pulse is

$$E_{\min,n} = \frac{2\log 2}{\pi} + \mathrm{O}\left(\frac{1}{n}\right). \tag{52}$$

A self refocused pulse is obtained by using the poles of $r_n(\xi)$ in the upper half plane to define bound states. The energy of the self refocused pulse is given by

$$E_{\mathrm{ref},n} = E_{\min,n} + \frac{4}{\sin(\pi/2n)} \approx \frac{2\log 2}{\pi} + \frac{8n}{\pi}. \tag{53}$$

Remark 5. In much of the MR-literature it is asserted that the energy of a selective pulse is proportional to the square of the flip angle. This is approximately true for small flip angles. For a selective pulse, producing a φ-flip for frequencies in a band of width B, formula (51) implies that the energy satisfies

$$E_{B,\varphi} \geqslant \frac{B}{\pi\gamma^2}\log\left(\frac{2}{1+\cos\varphi}\right). \tag{54}$$

Inversion and refocusing pulses are very important in all applications of MR. Such a pulse carries $[0,0,1]^\dagger$ to $[0,0,-1]^\dagger$. If this is the case at offset frequency ξ_0, then $r(\xi_0) = \infty$. It would therefore require infinite energy to exactly invert $[0,0,1]^\dagger$, for offset frequencies belonging to an interval of positive length. Formula (51) shows that the energy required to flip spins, with offset frequencies belonging to a band of width B, through an angle $\pi - \epsilon$, is at least

$$\frac{B}{\pi\gamma^2}\log\left(\frac{2}{1-\cos\epsilon}\right) \simeq \frac{2B}{\pi\gamma^2}\log\left(\frac{4}{\epsilon}\right). \tag{55}$$

Remark 6. If $r(\xi)$ is the reflection coefficient determined by $q(t)$, then, for $\lambda > 0$, $r(\lambda\xi)$ is the reflection coefficient determined by the potential $\lambda^{-1}q(\lambda^{-1}t)$. This is true, whether or not $q(t)$ has bound states, and agrees with the well-known heuristic principle that the effective support of the RF-envelope is inversely proportional to the bandwidth of excitation. It also shows that the maximum amplitude and energy of the RF-envelope are proportional to the bandwidth. The L^2-oscillation of the RF-envelope, $\int |q_t|^2\,\mathrm{d}t$, is proportional to the square of the bandwidth.

5. Inverse scattering for the ZS-system

There are several different approaches to solving the inverse scattering problem, stated in Section 3, see [1–3] or [6]. In this section we describe the solution of this problem via the Marchenko equations. We again follow the presentation in [1]. We generally suppose that the $\{\xi_j\}$ are *distinct* complex numbers with positive imaginary parts. This simplifies the exposition, though it is not necessary for the applicability of the inverse scattering method. To begin with, we assume that the reflection coefficient is smooth and rapidly vanishing at $\pm\infty$.

Given the reduced scattering data $\{r(\xi), \xi \in \mathbb{R}; (\xi_{\mathbb{1}}, C_1), \ldots, (\xi_{\mathbb{N}}, C_N)\}$, with $\xi_i \neq \xi_j$, for $i \neq j$, define the function

$$f(t) = \frac{1}{2\pi}\int_{-\infty}^{\infty} r(\xi)\mathrm{e}^{\mathrm{i}\xi t}\,\mathrm{d}\xi - i\sum_{j=1}^{N} C_j\mathrm{e}^{\mathrm{i}\xi_j t}. \tag{56}$$

This is the inverse Fourier transform of $r(\xi)$ with a correction added to account for the bound states. The finite sum in (56) is exponentially decreasing as t tends to $+\infty$. For each $t \in \mathbb{R}$, define the operator F_t by

$$F_t h(s) = \int_t^{\infty} f(s+y)h(y)\,\mathrm{d}y \text{ for } s \in [t,\infty). \tag{57}$$

We denote the adjoint of F_t, as an operator on $L^2([t,\infty))$, by F_t^*. For each $t \in (-\infty,\infty)$, the (right) Marchenko equation is the integral equation, for a function $k_t(s)$ defined for $s \in [t,\infty)$, given by

$$\left[\left(\mathrm{Id} + F_t^*F_t\right)k_t\right](s) = f^*(t+s), \tag{58}$$

or more explicitly

$$k_t(s) + \int_t^{\infty}\left[\int_t^{\infty} f^*(s+y)f(y+x)\,\mathrm{d}y\right]k_t(x)\,\mathrm{d}x = f^*(t+s). \tag{59}$$

The solution of the inverse scattering problem is given in the following theorem:

Theorem 3. *Given a smooth, rapidly decaying reflection coefficient $r(\xi)$, and a finite set of pairs $\{(\xi_j, C_j) : j = 1,\ldots,N\}$, with the $\{\xi_j\}$ distinct, $\mathrm{Im}\,\xi_j > 0$ and $C_j \neq 0$ for $j = 1,\ldots,N$, Eq.* (58) *has a unique solution for every $t \in \mathbb{R}$. If*

$$q(t) = -2k_t(t), \tag{60}$$

then the ZS-system, with this potential, has reflection coefficient r. It has exactly N bound states at frequencies $\{\xi_1,\ldots,\xi_N\}$, and the relations (34) *hold at these points.*

This theorem is proved in [2,6].

Remark 7. As the operator $(\mathrm{Id} + F_t^*F_t)$ is self adjoint and positive definite, it is an elementary fact that (58) has a unique solution. Since F_t is a compact operator, it is straightforward to numerically approximate this equation. We defer a discussion of the practicalities of solving (58) to Section 6. For the moment suffice it to say that this equation can be solved by a simple iteration, for values of t, such that

$$\int_{2t}^{\infty} |f(x)|\,\mathrm{d}x < 1. \tag{61}$$

There is also a "left" Marchenko equation, given in Section 6, where the integrals are over half lines of the form $(-\infty, t]$. In this formulation, the analogous finite sum of exponentials is decreasing as t tends to $-\infty$. Using both the left and right Marchenko equations, it is possible to obtain an algorithm for solving (59). In Sections 6 and 7 we give the foundations for this algorithm.

Remark 8. As noted above, there is a similar result if a has higher order zeros. In this case the definition of f needs to be modified; see [1].

The results of this section show that, at least in principle, the IST provides an infinite *dimensional space* of solutions to the RF-pulse synthesis problem. A practical magnetization profile has bounded support, and may be approximated by a smooth function. While the choice of approximation is a basic part of any practical pulse synthesis algorithm, we do not consider it systematically in this paper. This leaves the question of choosing the bound states to obtain an "optimal" RF-pulse envelope, which produces the desired magnetization profile. The notion of optimality depends on the intended application. It usually entails a balance among the amplitude, energy, duration, as well as the rephasing time. In the next two sections we give an algorithm, which allows for an arbitrary specification of bound states and norming constants.

6. Solving the Marchenko equation with small data

In this and the next section we discuss an algorithmic approach for finding potentials with a given magnetization profile and arbitrarily selected bound states. It entails using the right and left Marchenko equations, (58) and (67), respectively. In [17], Rourke and Morris consider several methods for solving the Marchenko equation. For small data they directly solve the (right) Marchenko equation. When incorporating bound states, they adapt a method of Moses and Proesser [12].

The method of Moses and Proesser is to approximate the reflection coefficient by a rational function with all of it poles *in the lower half plane*. This ensures that the resultant potential is supported in $(-\infty, 0]$, and has no bound states. In [17], this condition on the placement of the poles is removed. In Examples 2 and 3 Morris and Rourke [17], use rational approximations, $\{\tilde{r}_n(\xi)\}$, for $r(\xi)$ with poles in both half planes; the solutions they find are supported in $(-\infty, 0]$. However, the poles of $\tilde{r}_n(\xi)$ in the upper half plane force the resultant potential for the ZS-system to have bound states. On the one hand, the bound states increase the energy and amplitude of the RF-envelope, without affecting the magnetization profile. On the other hand, by using bound states, Morris and Rourke obtain truly self refocused pulses. Applying formula (50) to Example 2 of [17], we see that the energy required by the magnetization profile used in these examples (the integral in (50)) is 1.1. The energy resulting from bound states (the finite sum in (50)) is 2513 for $n = 20$, and 44,334 for $n = 84$.

We now present an algorithm to solve the Eq. (59) directly. The algorithm is described in the realm of continuum mathematics, but can be approximately implemented on a computer. This algorithm allows for the arbitrary specification of bound states, independently of the behavior of $r(\xi)$ off the real axis. Eq. (58) involves integration over positive rays. When the reflection coefficient is large, as is the case with an inversion pulse, or there are bound states, then the right Marchenko equation becomes ill conditioned as t tends to $-\infty$. In this case it is useful to work both ends against the middle. For that purpose we give the *left Marchenko equation*, which involves integration over negative rays. Conceptually, the left equation arises by doing scattering theory for Eq. (18) beginning with solutions normalized as $t \to +\infty$, instead of as $t \to -\infty$.

Recall that $r = b/a$; given r, and the locations of the bound states, we can use (40) to determine a, and therefore b. For $\xi \in \mathbb{R}$, define

$$\tilde{r}(\xi) = \frac{b^*(\xi)}{a(\xi)}, \tag{62}$$

and let $\{\xi_1, \ldots, \xi_N\}$ be the zeros of a in the upper half plane. The kernel function for the left Marchenko equation is defined by

$$g(t) = \frac{1}{2\pi}\int_{-\infty}^{\infty} \tilde{r}(\xi)\mathrm{e}^{-\mathrm{i}\xi t}\,\mathrm{d}t - \mathrm{i}\sum_{j=1}^{N} \widetilde{C}_j \mathrm{e}^{-\mathrm{i}\xi_j t}, \tag{63}$$

where the coefficients $\{\widetilde{C}_j\}$ are given by

$$\widetilde{C}_j = \frac{1}{C_j[a'(\xi_j)]^2}. \tag{64}$$

The finite sum of exponentials in (63) decays as t tends to $-\infty$. The values $\{a'(\xi_j)\}$ are easily computed using formula (40). It implies that

$$a'(\xi_k) = \frac{1}{\xi_k - \xi_k^*} \times \prod_{j\neq k}\left(\frac{\xi_k - \xi_j}{\xi_k - \xi_j^*}\right)\exp\left[\frac{\mathrm{i}}{2\pi}\int_{-\infty}^{\infty}\frac{\log(1+|r(\zeta)|^2)\,\mathrm{d}\zeta}{\zeta - \xi_k}\right]. \tag{65}$$

If the bound states are close together, then $|a'(\xi_k)|^2$ may become quite small; this, in turn, makes $\widetilde{C}_j$ quite large. So even though the exponentials in (63) decay rapidly as $t \to -\infty$, the finite sum in (63) can be very large for t near to zero. We consider this further in the next section.

For each $t \in \mathbb{R}$, define an operator from $L^2((-\infty, t])$ to itself by

$$G_t l(s) = \int_{-\infty}^{t} g(s+y) l(y)\,\mathrm{d}y. \tag{66}$$

For each $t \in \mathbb{R}$, the left Marchenko equation is

$$\left[\left(\mathrm{Id} + G_t G_t^*\right) l_t\right](s) = -g(s+t), \text{ for } s \in (-\infty, t], \tag{67}$$

or more explicitly

$$l_t(s) + \int_{-\infty}^{t} \left[\int_{-\infty}^{t} g(s+y) g^*(y+x)\,\mathrm{d}y\right] l_t(x)\,\mathrm{d}x = -g(s+t). \tag{68}$$

If $l_t(s)$ solves this equation, then the potential defined by

$$q(t) = 2l_t(t), \tag{69}$$

has reflection coefficient $r(\xi)$. It has exactly N bound states located at frequencies $\{\xi_1, \ldots, \xi_N\}$, and the relations (34) hold at these points. In principle, the potential could be recovered from the reduced scattering data using either Eq. (58) or (67), alone. As a practical matter, there is a τ_0 (which depends on the scattering data) such that a much more stable algorithm follows by using Eq. (58) to determine $q(t)$ for $t \geqslant \tau_0$ and Eq. (67), to determine $q(t)$ for $t < \tau_0$.

Eq. (67) can be derived from (58) by considering the scattering theory for the "time reversed" potential

$$q_-(t) = -q(-t). \tag{70}$$

For example, it is not difficult to show that the reflection coefficient for q_- is

$$r_-(\xi) = -\frac{b(-\xi)}{a^*(-\xi)}. \tag{71}$$

A detailed derivation can be found in [6]. In most of our analysis we concentrate on the right Marchenko equation, (58), with the understanding that everything said applies, *mutatis mutandis*, to the left formulation as well. Using both equations leads to a practical method for finding q.

Remark 9. Using Eqs. (60), (69), and (71) it is not difficult to show that a real pulse is even ($q(t) = q(-t)$) if and only if $b(\xi)$ is real valued.

We give two rather different, constructive existence results for solutions to Eqs. (58) and (67). The first result is for large $|t|$ (or small data) and includes a very precise pointwise bound for $|q(t)|$ in this domain. This is useful for assessing the effective support of the potential. The other result is an existence result that is valid for all times. Define the functions:

$$\begin{aligned} M_f(t) &= \sup_{s \geqslant t} |f(s)|, \quad I_f(t) = \int_t^{\infty} |f(s)|\,\mathrm{d}s, \\ M_g(t) &= \sup_{s \leqslant t} |g(s)|, \quad I_g(t) = \int_{-\infty}^{t} |g(s)|\,\mathrm{d}s. \end{aligned} \tag{72}$$

We say that the right, resp. left, Marchenko equation can be solved by *simple iteration* on the interval $[t, \infty)$, resp. $(-\infty, t]$, if the sequence defined by

$$\begin{aligned} &k_t^0(s) = f^*(s+t), \;\; k_t^j(s) = f^*(s+t) - F_t^* F_t k_t^{j-1}(s), \;\; j = 1,2,\ldots \\ &\text{resp.,} \\ &l_t^0(s) = -g(s+t), \;\; l_t^j(s) = -g(s+t) - G_t G_t^* l_t^{j-1}(s), \;\; j = 1,2,\ldots, \end{aligned} \tag{73}$$

converges uniformly to $k_t(s)$ for $s \in [t, \infty)$, resp. to $l_t(s)$ for $s \in [-\infty, t]$.

Remark 10. In [17], Morris and Rourke solve the right Marchenko equation in several different ways. For small data they use an algorithm based on the iteration defining $\{k_t^j(s)\}$, given in (73).

Theorem 4. *If $I_f(2t) < 1$, resp., $I_g(2t) < 1$, then the right, resp. left, Marchenko equation, can be solved by simple iteration on the interval $[t, \infty)$, resp. $(-\infty, t]$. The solutions satisfy the estimates*

$$\begin{aligned} |k_t(s)| &\leqslant \frac{M_f(2t)}{1 - I_f^2(2t)}, \text{ for } s \in [t, \infty), \\ |l_t(s)| &\leqslant \frac{M_g(2t)}{1 - I_g^2(2t)}, \text{ for } s \in (-\infty, t]. \end{aligned} \tag{74}$$

The proof is given in the Appendix A. Note that no assumption is made concerning the presence or absence of bound states.

The estimates in (74) imply that, so long as the hypotheses of the theorem hold, the potential $q(t)$ satisfies the estimates

$$|q(t)| \leqslant \frac{2M_f(2t)}{1 - I_f^2(2t)}, \text{ or } |q(t)| \leqslant \frac{2M_g(2t)}{1 - I_g^2(2t)}. \tag{75}$$

This shows that the growth and support of $q(t)$ are determined by those of f and g. In Fig. 4 we compare the magnitude of the minimum energy 140° IST pulse (with a 25% transition window) to $\min\{(2M_f(2t))/(1 - I_f^2(2t)), (2M_g(2t))/(1 - I_g^2(2t))\}$. This plot shows that the bound derived in Theorem 4 gives a very good estimate for both the support and growth of q. These estimates show that, when studying the effects on the support of $q(t)$, of using different approximations for $r(\xi)$, or the addition of bound states, it suffices to work with $f(t)$ and $g(t)$. It is not necessary to actually solve the Marchenko equations.

7. Solving the Marchenko equation with large data

If $I_f(t) \geqslant 1$ then we may need to modify the iteration, defined above, to find a solution to Eq. (58). In this section we present a theoretical algorithm, for solving the Marchenko equations, which does not require any smallness assumptions. Given any reflec-

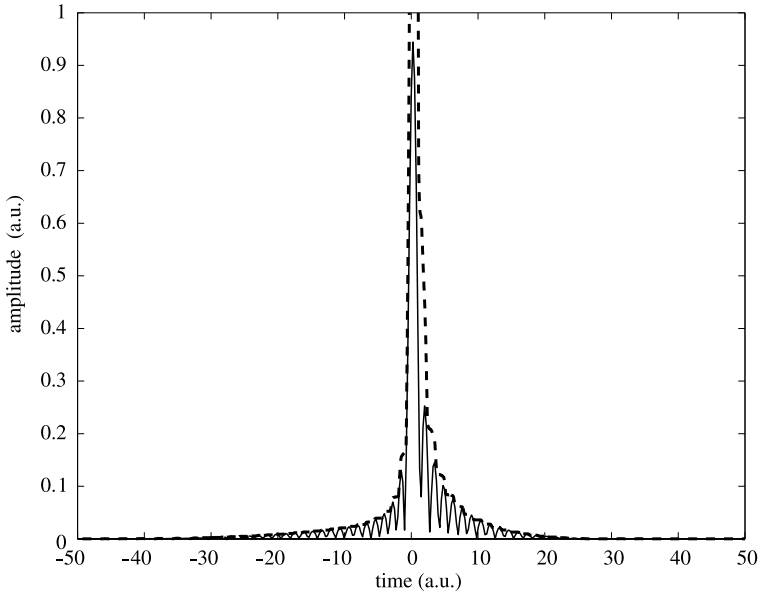

Fig. 4. A graph of the magnitude of the minimum energy 140° IST pulse having a 25% transition zone (solid line) and of $\min\{(2M_f(2t))/(1-I_f^2(2t)),(2M_g(2t))/(1-I_g^2(2t))\}$ (dashed line).

tion coefficient and choice of bound states, this algorithm could, in principle, be used to find the potential. For certain applications it has proven to be very slow, and not sufficiently accurate. We include this material for mathematical completeness, and because it reveals certain special properties of the Marchenko equations in this case. In collaboration with Jeremy Magland, we have recently found a very fast and stable approach for solving the left and right Marchenko equations; it will be the subject of a future joint publication.

We start with an L^2-norm estimate for F_t.

Lemma 1. *If $f \in L^1([t,\infty))$ then, for every $h \in L^2([t,\infty))$ we have the estimate*

$$\|F_t h\|_{L^2([t,\infty))} \leqslant I_f(2t)\|h\|_{L^2([t,\infty))}. \tag{76}$$

The proof is in the Appendix A.

The fact that $I_f(2t) = I_{f^*}(2t)$, and the lemma imply that

$$\|F_t^* F_t h\|_{L^2([t,\infty))} \leqslant I_f(2t)\|F_t h\|_{L^2([t,\infty))} \leqslant I_f(2t)^2\|h\|_{L^2([t,\infty))}. \tag{77}$$

To simplify the notation we set $\gamma_t = I_f(2t)^2$. As a map from $L^2([t,\infty))$ to itself, $F_t^* F_t$ is a self adjoint, positive operator. The estimate in (77) implies that its spectrum lies in $[0,\gamma_t]$, and therefore the spectrum of $\left(F_t^* F_t - \frac{\gamma_t}{2}\mathrm{Id}\right)$ lies in $\left[-\frac{\gamma_t}{2},\frac{\gamma_t}{2}\right]$. The norm of $\left(F_t^* F_t - \frac{\gamma_t}{2}\mathrm{Id}\right)$ is therefore, at most, $\gamma_t/2$. We rewrite Eq. (59) in the form

$$\left[\mathrm{Id} + \frac{2}{2+\gamma_t}\left(F_t^* F_t - \frac{\gamma_t}{2}\mathrm{Id}\right)\right] k_t = \frac{2}{2+\gamma_t} f^*(t+s). \tag{78}$$

The norm of the operator $(2/(2+\gamma_t))(F_t^* F_t - \frac{\gamma_t}{2}\mathrm{Id})$ is less than $\gamma_t/(2+\gamma_t)$, which is, in turn, less than 1. Eq. (78) can therefore be solved by iteration. We define a new iteration by setting

$$\begin{aligned}\tilde{k}_t^0(s) &= \frac{\gamma_t}{2+\gamma_t} f^*(s+t),\\ \tilde{k}_t^j(s) &= \frac{\gamma_t}{2+\gamma_t}\left(f^*(s+t) - \left(F_t^* F_t - \frac{\gamma_t}{2}\mathrm{Id}\right)\tilde{k}_t^{j-1}\right).\end{aligned} \tag{79}$$

We have the following convergence result.

Proposition 1. *If $f \in L^1([2t,\infty))$ then the sequence defined in* (79) *converges in $L^2([t,\infty)$ to the solution of Eq.* (58).

Proof. This statement is an immediate consequence of the fact that the L^2-norm of the operator $(\gamma_t/(2+\gamma_t))(F_t^* F_t - \frac{\gamma_t}{2}\mathrm{Id})$ is less than 1. □

Remark 11. If $\partial_x f(x)$ also belongs to $L^1([2t,\infty))$, then the solution converges locally uniformly to the unique solution of (58). While this statement is not difficult to prove it requires mathematical techniques beyond the scope of this paper.

Remark 12. We can apply the same reasoning to the left Marchenko equation. Set $\delta_t = I_g(2t)^2$. Eq. (67) is equivalent to

$$\begin{aligned}&\left[\mathrm{Id} + \frac{2}{2+\delta_t}\left(G_t G_t^* - \frac{\delta_t}{2}\mathrm{Id}\right)\right] l_t\\ &\quad = -\frac{2}{2+\delta_t} g(t+s).\end{aligned} \tag{80}$$

On $L^2((-\infty,t])$, the operator $(2/(2+\delta_t))(G_tG_t^* - \frac{\delta_t}{2}\mathrm{Id})$ has norm less than $\delta_t/(2+\delta_t)$. Thus, the sequence

$$\begin{aligned}\tilde{l}_t^0(s) &= -\frac{\delta_t}{2+\delta_t}g(s+t),\\ \tilde{l}_t^j(s) &= -\frac{\delta_t}{2+\delta_t}\left(g(s+t)+\left(G_tG_t^* - \frac{\delta_t}{2}\mathrm{Id}\right)\tilde{l}_t^{j-1}\right)\end{aligned} \tag{81}$$

converges, in $L^2((-\infty,t])$, to the solution of (67).

Remark 13. In some of the examples in this paper, we have simply discretized the Marchenko equations, and used the iteration schemes defined in Eqs. (79) and (81) to find $\{k_{t_j^+}(t_j^+)\}$ and $\{l_{t_j^-}(t_j^-)\}$. For these iterative algorithms, the size of the error at iterate n is proportional to $\left(1+\frac{2}{\gamma_t}\right)^{-n}$ or $\left(1+\frac{2}{\delta_t}\right)^{-n}$.

As remarked above, when the bound states bunch together, the left norming constants, $\{\widetilde{C}_j\}$, can become quite large. If the left norming constants are large then, as t approaches τ_0, γ_t, and δ_t become quite large, and these iteration schemes converge very slowly. This approach could likely be improved by using preconditioning. However, we do not pursue this further, for, as noted above, we have, in collaboration with Jeremy Magland, found a much faster and more stable method for solving the Marchenko equations.

8. Comparison with the Shinnar–LeRoux method

In this section, the function $r_i(\xi)$, is the reflection coefficient defined by an "ideal" magnetization profile, $\boldsymbol{m}_i^\infty$, as in Eq. (44). A good example to keep in mind is a φ-flip for offset frequencies in $[-w,w]$; the corresponding reflection coefficient is

$$r(\xi) = \begin{cases} \frac{\sin\varphi}{1+\cos\varphi} & \text{for } \xi \in \left[-\frac{w}{2},\frac{w}{2}\right],\\ 0 & \text{for } \xi \notin \left[-\frac{w}{2},\frac{w}{2}\right].\end{cases} \tag{82}$$

The foundation of the Shinnar–Le Roux (SLR) algorithm is the *hard pulse approximation*. In this approach one designs a potential of the form

$$q_0(t) = \sum_{j=1}^{N}\mu_j\delta(t-j\Delta), \tag{83}$$

to produce an approximation to the ideal magnetization profile for v in a subinterval of

$$[-\Delta^{-1}\pi,\Delta^{-1}\pi]. \tag{84}$$

A potential like $q_0(t)$ presents no special difficulties for the forward scattering analysis presented in Section 3. In this case the scattering matrix takes the special form

$$s(\xi) = \begin{bmatrix} \mathrm{e}^{\mathrm{i}N\Delta\xi}A_0(\mathrm{e}^{-\mathrm{i}\Delta\xi}) & \mathrm{e}^{\mathrm{i}N\Delta\xi}B_0^*(\mathrm{e}^{-\mathrm{i}\Delta\xi})\\ \mathrm{e}^{-\mathrm{i}N\Delta\xi}B_0(\mathrm{e}^{-\mathrm{i}\Delta\xi}) & -\mathrm{e}^{-\mathrm{i}N\Delta\xi}A_0^*(\mathrm{e}^{-\mathrm{i}\Delta\xi})\end{bmatrix}, \tag{85}$$

where $A_0(z)$ and $B_0(z)$ are polynomials of degree $N-1$. The reflection coefficient $r_0(\xi)$, defined by $q_0(t)$, is the *periodic* function of period $\Delta^{-1}2\pi$ given by

$$r_0(\xi) = \frac{\mathrm{e}^{-2\mathrm{i}N\Delta\xi}B_0(\mathrm{e}^{-\mathrm{i}\Delta\xi})}{A_0(\mathrm{e}^{-\mathrm{i}\Delta\xi})}. \tag{86}$$

The SLR algorithm has two parts: (1) Find polynomials of the given degrees, so that $r_0(\xi)$ is, in a certain sense, an approximation to $r_i(\xi)$. (2) Use a recursive method for determining the coefficients, $\{\mu_j\}$, so that $q_0(t)$, given in (83), has reflection coefficient $r_0(\xi)$. Of course, a sum of δ-pulses is nonphysical, requiring infinite energy to realize. The RF-envelope that is actually used is a "softened" version of $q_0(t)$. For example, one could replace each $\mu_j\delta(t-j\Delta)$ by a boxcar pulse of width Δ with the same area, leading to the softened pulse

$$q_1(t) = \sum_{j=1}^{N}\frac{\mu_j}{\Delta}\chi_{[0,\Delta)}(t-j\Delta). \tag{87}$$

While the difference $q_0(t)-q_1(t)$ can only be made small in the sense of generalized functions, the difference $|r_0(\xi)-r_1(\xi)|$ can be made pointwise small, for ξ in a fixed interval, provided that none of the $\{\mu_j\}$ is too large. This is what is usually meant by the "hard pulse approximation," see [19,22].

Beyond the details of algorithmic implementations, there are three principal differences between the IST method outlined above, and the SLR approach. The first is that, in the IST approach, one is free to specify the locations of the bound states and norming constant, entirely independently of the reflection coefficient on the real axis. In SLR, one is very constrained in both the locations of the bound states, and the norming constants. Moreover, these constraints are of a rather implicit nature. The second major difference is that, in IST, a pulse is designed using the magnetization profile, whereas in SLR, it is designed using the flip angle profile. The third difference is that, in SLR, the duration of the pulse is essentially specified in advance. It should be fairly clear that one cannot simultaneously specify the magnetization profile, *and* the duration, of the pulse. This is certainly the case for minimum energy pulses. Indeed, the second and third differences are intimately related. In order to be able to specify the pulse duration, in the SLR approach, direct control over the *phase* of the magnetization profile is sacrificed. To illustrate the relationship between pulse duration, and the phase of the magnetization profile we consider the example of a minimum energy 90° SLR-pulse. We follow the presentation of SLR given in [14].

Suppose that the ideal reflection coefficient is

$$r_i(\xi) = \frac{b(\xi)}{a(\xi)} = \begin{cases} 1 & \text{for } \xi \in [-1,1], \\ 0 & \text{for } \xi \notin [-1,1], \end{cases} \tag{88}$$

with $|a(\xi)|^2 + |b(\xi)|^2 = 1$, and $a(\xi)$ analytic in the upper half plane. Note that the flip angle at offset ξ is given by $2\sin^{-1}(|b(\xi)|)$. A polynomial, $B_0(z)$, of degree $N-1$, is found so that $B_0(e^{-i\Delta\xi})$ has linear phase, and $|B_0(e^{-i\Delta\xi})|$ approximates $|b(\xi)|$ over the interval $[-\Delta^{-1}\pi, \Delta^{-1}\pi]$. If one specifies tolerances on the in-slice, and out-of-slice ripple, then the transition width is essentially an output of the algorithm. Because $|B_0(e^{-i\Delta\xi})|$ is designed as an approximation to $|b(\xi)|$ rather than $B_0(e^{-i\Delta\xi})$ as an approximation to $b(\xi)$, it is at this juncture that direct control over the phase of $r_0(\xi)$ is lost.

The next step is the determination of $A_0(z)$; it must be a polynomial of degree $N-1$ such that

$$|A_0(z)|^2 + |B_0(z)|^2 = 1, \text{ if } |z| = 1. \tag{89}$$

There are many possible choices, which are labeled, in essence, by the locations of the zeros of $A_0(z)$. The minimum energy SLR pulse is obtained by taking the zeros of $A_0(z)$ to lie inside the unit disk. In this case $A_0(z)$ is determined by the condition that $\log|A_0(z)|$ and $\arg A_0(z)$ are a Hilbert transform pair for $|z| = 1$. Noting that $|A_0(z)| = \sqrt{1 - |B_0(z)|^2}$, we see that $r_0(\xi)$, as defined in Eq. (86), is not an approximation to $r_i(\xi)$, but rather an approximation to $e^{-2i\tau\xi} r_{\mathrm{SLR}}(\xi)$, where

$$r_{\mathrm{SLR}}(\xi) = \frac{|b(\xi)|}{a(\xi)} = \frac{|b(\xi)|}{b(\xi)} r_i(\xi). \tag{90}$$

As noted in Section 3, the linear phase, $2\tau\xi$, corresponds to shifting $q_0(t)$ in time by τ-units. While the allowable in-slice and out-of-slice ripple, and therefore the transition width, make some contribution to the control of the duration of an SLR pulse, (especially for very short pulses), the possibility of specifying the duration comes from choosing $|B_0|$ as an approximation to $|b|$ rather than B_0 as an approximation to b.

Fig. 5A shows $r_i(\xi)$ (which is real) as well as the real and imaginary parts of $r_{\mathrm{SLR}}(\xi)$ (defined in Eq. (90)) for a 90° pulse. Fig. 5B shows the phase of $r_{\mathrm{SLR}}(\xi)$. Near the middle of the passband, it is well approximated by a linear function, and therefore, most of the phase error produced by $q_0(t)$ can be removed by using a slightly longer rephasing time. Fig. 6 shows both the absolute values of the transverse magnetization, and the transverse magnetization for three 90° SLR pulses. Because $m_3 = 0$ for a 90°-flip, these are essentially plots of $|r_0(\xi)|$ and $r_0(\xi)$, respectively. Each pulse has a 1KHz bandwidth, and 1% in-slice and out-of-slice ripple. The pulses have durations of 10, 20, and 30 ms, respectively. The selectivity of the pulse increases somewhat as the duration increases. For each pulse, the rephasing has been adjusted to get the minimum phase error in the passband. But for the additional rephasing, which flattens the magnetization profile near the center of the window, as the pulse duration increases, the magnetization profile becomes a better and better approximation to the function $r_{\mathrm{SLR}}(\xi)$, shown in Fig. 5A. Finally, the plots in Figs. 7A and B show the same information for a 1 kHz, minimum energy 90° IST pulse, having essentially the same ripple, and transition width as the 10 ms SLR pulse. The IST pulse is shown in Fig. 7C; note that the IST pulse produces essentially no phase error, but has a duration of about 16 ms. It should also be noted that this IST pulse has a rephasing time very close to that of the 10 ms SLR pulse.

Tracing back through the computations, we see that the phase of $r_{\mathrm{SLR}}(\xi)$ is determined by the Hilbert transform of $\log(1 + |r_i(\xi)|^2)$. It is the more or less accidental fact that this function is close to linear, within the support of $r_i(\xi)$, which allows the SLR design procedure to produce a pulse, with a specified duration, which can be rephased to give a reasonably good, *coherent* 90°-flip over the specified band.

The phase of B_0 is sometimes determined by other considerations. Above we used the linear phase condition, other common choices are the "minimum or maximum" phase conditions. In all cases, the reflection coefficient produced by the potential, is an approximation to $e^{i\phi(\xi)} r_i(\xi)$, for a nonconstant *and* nonlinear function $\phi(\xi)$. It is fortuitous that, in many instances, $\phi(\xi)$ is approximately linear over the support of $r_i(\xi)$, and, therefore, by adjusting the rephasing time, one can still attain a final magnetization close to the ideal. It also advantageous that small errors in the phase of the excitation often lead only to a minor decrease in the signal strength. This may not be the case for composite pulses, where the phase errors can accumulate, leading to significant signal loss. When using nonFourier encoding schemes, e.g., wavelets, it may be advantageous to use an approach that gives direct control over the phase of the excitation.

We close this section by briefly returning to the question of bound states in the SLR approach. The bound states correspond to the zeros of $A_0(z)$ for $|z| > 1$. Let $\{z_1, \ldots, z_{N-1}\}$ be the zeros of the minimum phase solution to (89), $A_{\min,0}(z)$. The other solutions to Eq. (89) are in two-to-one correspondance with the subsets of the set $\{1, \ldots, N-1\}$: Let $\boldsymbol{I} = \{1 \leqslant i_1 < \ldots < i_l \leqslant N-1\}$ be such a subset, and define

$$A_{\boldsymbol{I},\pm,0}(z) = \pm A_{\min,0}(z) \prod_{j=1}^{l} \left(\frac{1 - z_{i_j}^* z}{z - z_{i_j}} \right). \tag{91}$$

We observe that this is a polynomial of degree $N-1$ and that, if $|z| = 1$, then $|A_{\boldsymbol{I},\pm,0}(z)| = |A_{\min,0}(z)|$. Therefore, each $A_{\boldsymbol{I},\pm,0}(z)$ is also a solution to (89). Using the second part of the SLR algorithm, we can use $(A_{\boldsymbol{I},\pm,0}, B_0)$ to design pulses having the same flip angle profile as the minimum energy pulse described above. These pulses have larger energy, and their reflection coefficients have different phases

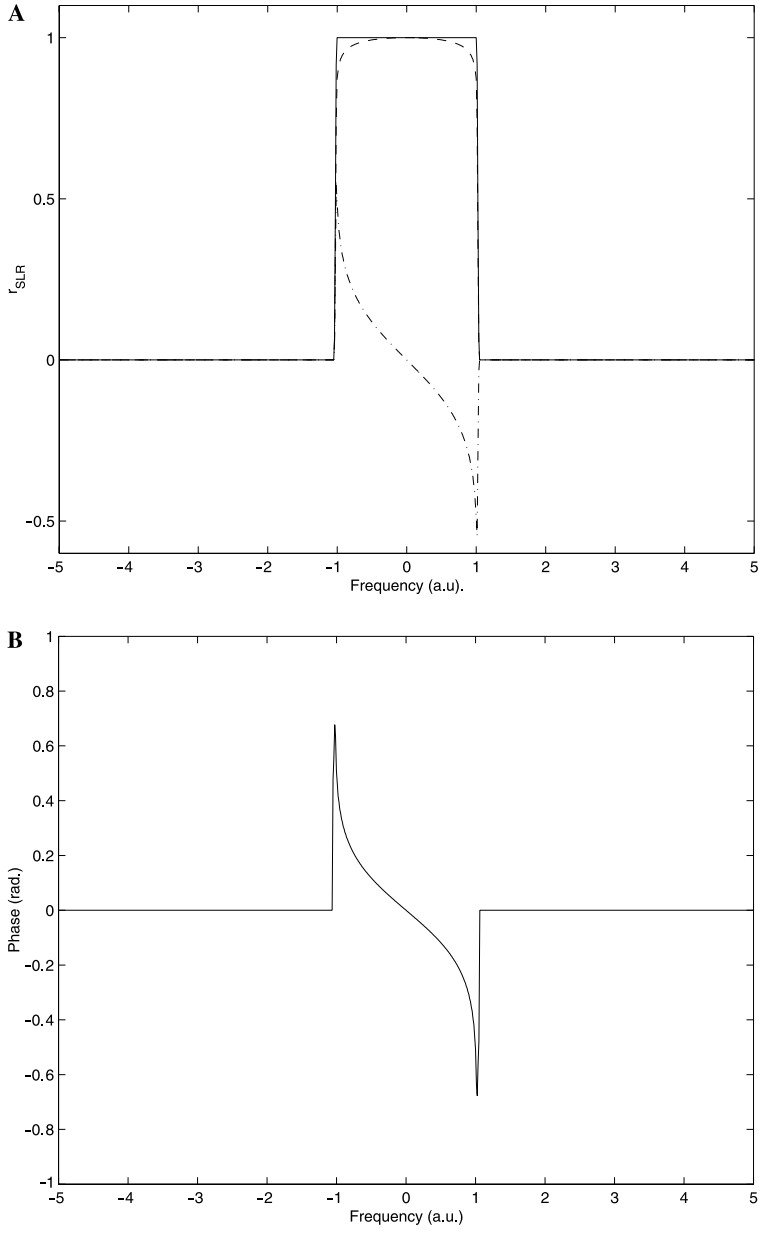

Fig. 5. Plots showing the phase error introduced in the SLR design process. (A) This plot shows the ideal reflection coefficient for a 90°-pulse (solid line), as well as the real (dashed line), and imaginary (dot-dash line) parts of the actual "ideal" reflection coefficient, $r_{\mathrm{SLR}}(\xi)$ used in the design of the minimum energy SLR pulse. (B) This plot shows the phase of $r_{\mathrm{SLR}}(\xi)$. Near the center of the passband, it is well approximated by a linear function; this makes it possible to largely remove the *designed in* phase error.

$$r_{\boldsymbol{I},\pm,0}(\xi) = \pm r_{\min,0}(\xi) \prod_{j=1}^{l} \left(\frac{1 - z_{i_j}^{*} \mathrm{e}^{-\mathrm{i}\Delta\xi}}{\mathrm{e}^{-\mathrm{i}\Delta\xi} - z_{i_j}} \right). \tag{92}$$

This indicates the constraints one encounters when introducing bound states in the SLR approach, at least using the method outlined in [14]. In [16] and [15], Pickup et al. observed that moving zeros of A_0, in the manner described above, increases the total energy of the pulse. This is consistent with formula (50), as, under the mapping $\xi \leftrightarrow z = \mathrm{e}^{-\mathrm{i}\Delta\xi}$, the exterior of the unit disk, in the SLR approach, corresponds to the upper half plane, in inverse scattering theory.

9. Practical aspects of IST pulse design

In this section we outline the steps required to design a usable pulse with the inverse scattering transform, and give several examples of pulses. This discussion is meant to be illustrative rather than prescriptive; we will return to these questions in a later publication.

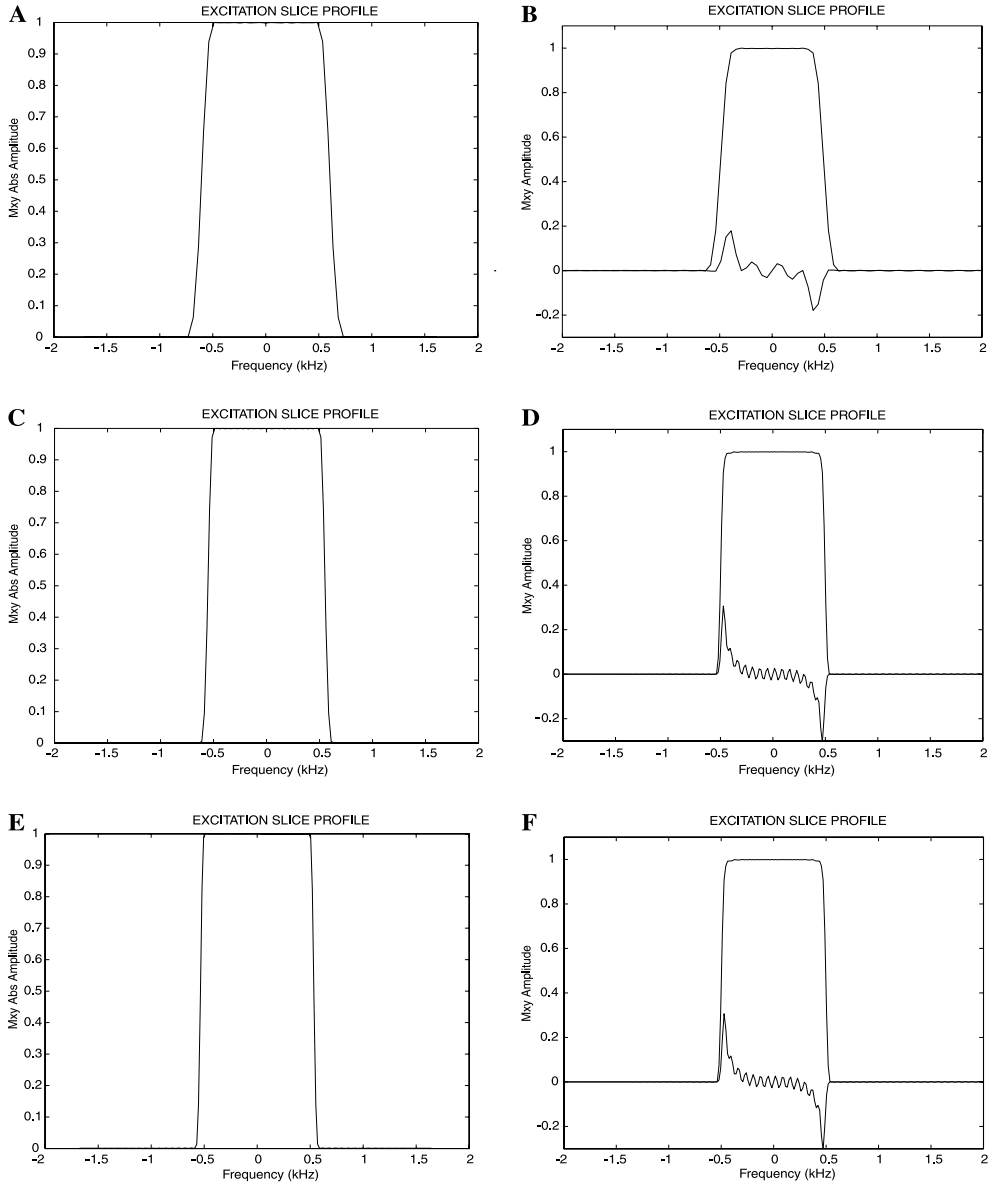

Fig. 6. These are the magnetization profiles produced by 1 kHz 90° minimum energy SLR pulse with 1% in-slice and out-of-slice ripple, and the indicated durations. These figures show the effects of changing the duration of an SLR pulse on the resulting transverse magnetization. (The SLR-pulses and magnetization profiles were produced using matpulse-2.4 by Gerald Matson and Mark Elliott [11].) (A) Ten milliseconds, absolute transverse magnetization; (B) 10 ms, transverse magnetization; (C) 20 ms, absolute transverse magnetization; (D) 20 ms, transverse magnetization; (E) 30 ms, absolute transverse magnetization; and (F) 30 ms, transverse magnetization.

The input to the IST pulse design process is an ideal magnetization profile, $\boldsymbol{m}^{\infty}(v)$, which, via Eq. (44), defines an ideal reflection coefficient $r_i(\xi)$. Frequently, the ideal reflection coefficient is a discontinuous function, see, e.g., Eq. (82).

1. The first step in IST pulse synthesis is to choose a smooth function with bounded support, $r_d(\xi)$, which is an approximation to $r_i(\xi)$. So far as the algorithm is concerned, the choice of approximation, $r_d(\xi)$, is constrained only by the need to have its Fourier transform, $\hat{r}_d(t)$, decay reasonably quickly. There is no need to use any special type of function such as a rational or meromorphic function. As with SLR pulse design, the "transition width," and ripple directly effect the duration of the final pulse.
2. The next step is to choose the locations of the bound states and the norming constants, $\{(\xi_1, C_1), i = 1, \ldots, N\}$. For a minimum energy pulse, no bound states are used. For a self refocused pulse, $r_d(\xi)$ is usually taken to be a rational function with simple poles. The $\{\xi_j\}$ are then the poles of $r_d(\xi)$ in the upper half plane, and the $\{C_j\}$ are the residues of $r_d(\xi)$ at these poles.
3. Given the data $\{r_d(\xi); (\xi_1, C_1), \ldots, (\xi_N, C_N)\}$, we determine the left reflection coefficients and left

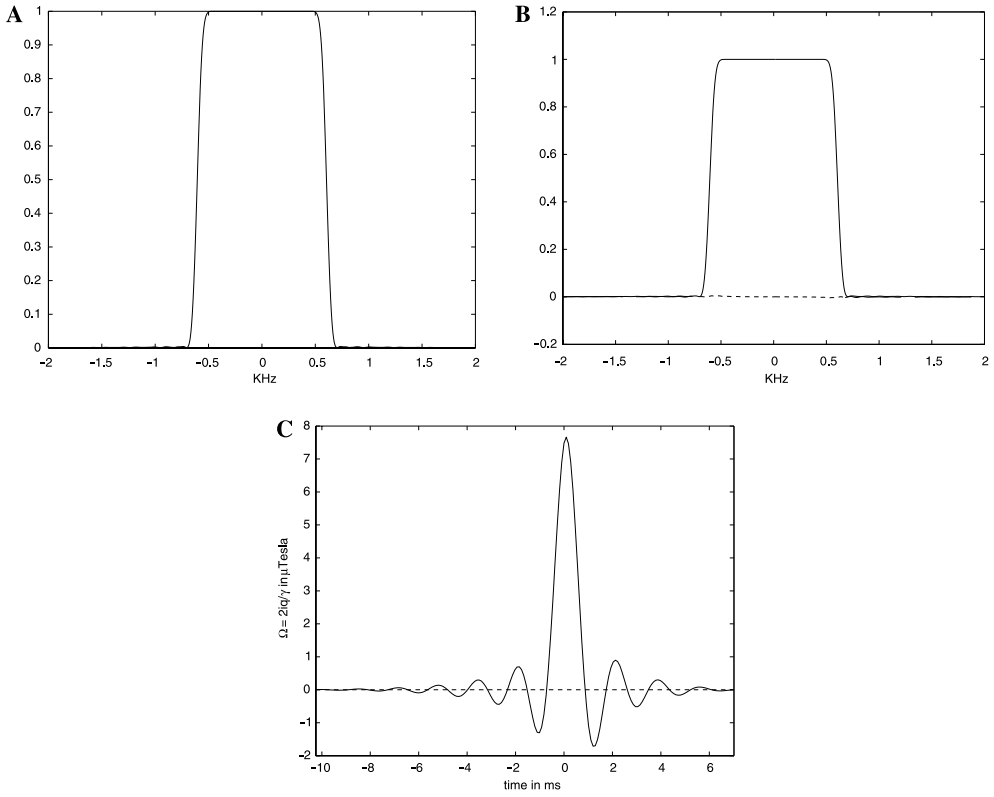

Fig. 7. For comparison with Figs. 6 (A, B), plots (A) and (B) show the absolute transverse magnetization, and transverse magnetization for the minimum energy 1 kHz, 90° IST pulse with a transition width, and ripple comparable to the 10 ms SLR pulse. Plot (C) shows the pulse, indicating a duration of about 16 ms, and a rephasing time of 6.5 ms. (A) Absolute transverse magnetization. (B) Transverse magnetization. (C) Pulse profile for a minimum energy 90° IST pulse.

norming constants, using Eqs. (62) and (64), respectively. With this data we can now determine the kernel functions, f and g, for the right and left Marchenko equations, using Eqs. (56) and (63), respectively. In practice these functions are computed at sample points by using the FFT. The functions $M_f(t)$ and $M_g(t)$ are computed (see Eq. (72)), the "switching" time τ_0 is determined as the unique solution to the equation $M_f(\tau_0) = M_g(\tau_0)$.

4. The left and right Marchenko equations are approximately solved to determine $\{q_d(t_j)\}$ at sample points $\{t_j\}$ belonging to a sufficiently large interval $[t^-, t^+]$. This interval should contain the effective support of $q_d(t)$, which can be determined, a priori, by using the estimates in (75). The right equation is used for $t_j \geqslant \tau_0$ and the left equation for $t_j < \tau_0$. The fineness of the sample spacing, Δ, is determined by the range of offset frequencies present in the sample. For, as is well known, using a sum of boxcar pulses of duration Δ to approximate $q_d(t)$, produces sidelobes in the magnetization profile at intervals of length $2\Delta^{-1}\pi$.
5. The duration of the pulse produced by the IST (i.e., the effective support of $q_d(t)$) may exceed what is allowable in the given application. In this case the pulse is truncated, and usually windowed with a smoothing function, e.g., $\cos^2(B(t - t_0))$. This leads to changes in the excitation profile, usually a decrease in selectivity as well as phase errors, see Fig. 3. Sometimes a better result is obtained by starting over, replacing $r_d(\xi)$ by a "smoother" function, i.e., a function with a wider transition region.

We now give some illustrative examples of pulses, designed using the IST, along with the transverse magnetization profiles they produce. In the transverse magnetization profiles, $m_1(v)$ is shown with a solid line, and $m_2(v)$ with a dashed line. With the exception of Example 4, in the pulse plots, $\omega_1(t)$ is shown with a solid line, while $\omega_2(t)$ is shown with a dashed line.

9.1. The details of the design of a 90°-flip

We start by giving the details of the design process for a minimum energy, 90° flip.

Example 2. The ideal reflection coefficient is given by formula (88). We approximate $r_i(\xi)$ by $r_d(\xi)$, a three times differentiable, piecewise polynomial function with support equal to $[-1.2, 1.2]$. This function is shown as the solid line in Fig. 8D. The kernel functions for the right and left Marchenko equations are shown in Figs.

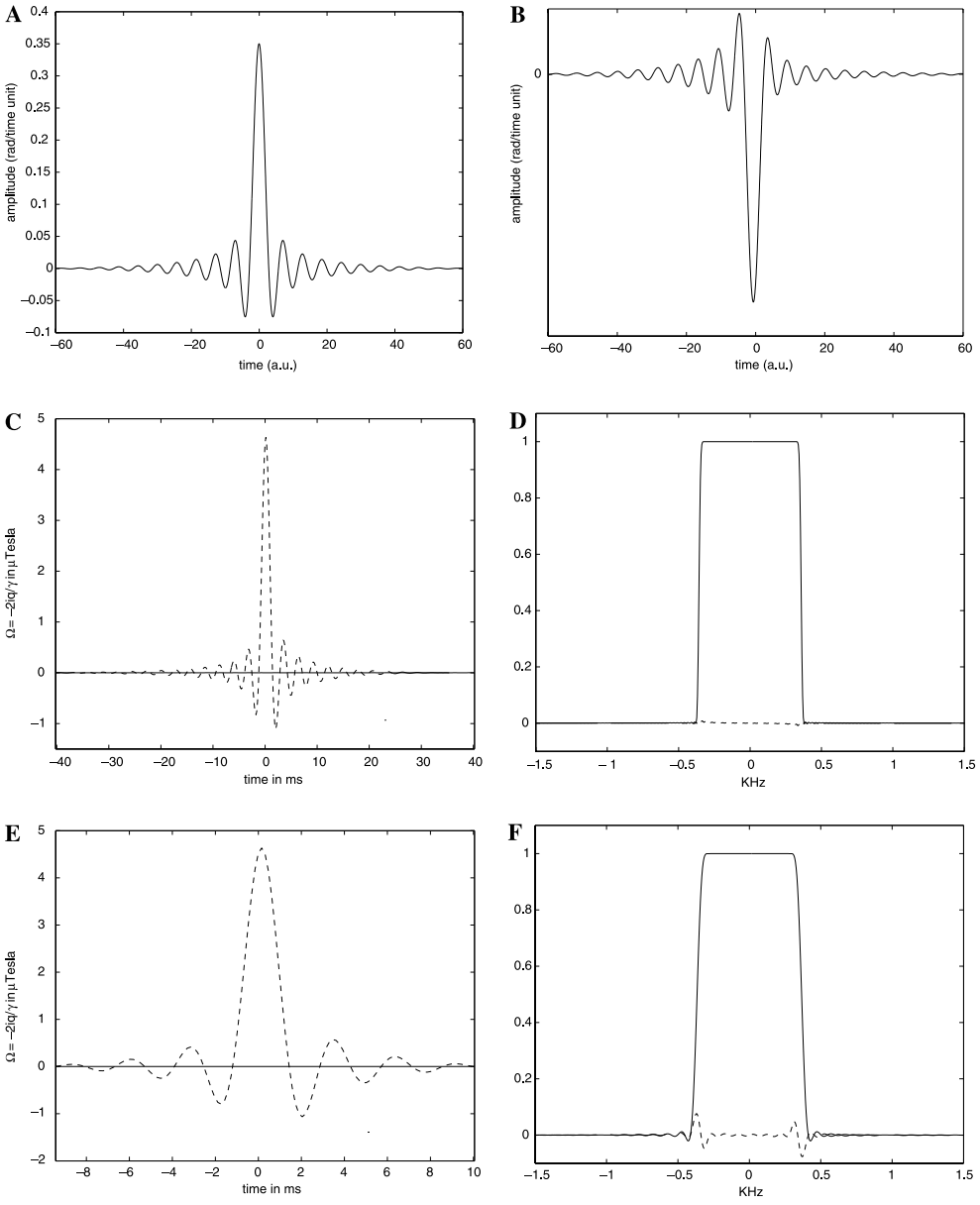

Fig. 8. The steps of the IST design process for a minimum energy 90° pulse. (A) f, the kernel function for the right Marchenko equation. (B) g, the kernel function for the left Marchenko equation. (C) The potential $q_d(t)$. (D) The transverse magnetization produced by $q_d(t)$. This is also a plot of $r_d(2\xi)$. (E) A smoothly windowed version of $q_d(t)$. (F) The transverse magnetization produced by the windowed potential shown in (E).

8A and B and the potential $q_d(t)$ (within its effective support) is shown in Fig. 8C. The Marchenko equations were solved using the simple iteration scheme described in Section 6. It required about 2 min on a 2 GHz Pentium Linux box to determine q_d at 830 points.

The transverse magnetization produced by $q_d(t)$ is shown in Fig. 8D. Fig. 8E shows a $\cos^2$-truncated version of q_d, and Fig. 8F shows the transverse magnetization it produces. As expected, the truncated pulse is somewhat less selective, and has some phase error. It is notable that the phase error produced by truncating an IST pulse is quite different from the phase error that arises in an SLR pulse with a similar duration and absolute magnetization profile. In most of the examples we have computed, the phase error, which results from smoothly windowing an IST pulse, is concentrated in the transition region.

9.2. The effect of adding bound states

In these examples we demonstrate the flexibility of the IST method with regard to the inclusion of bound states. These potentials were found using Magland's algorithm.

Example 3. In this example we show that the data used to define the bound states is independent of the reflection coefficient. For $r_d(\xi)$ we use the piecewise polynomial reflection coefficient defined in the previous example. This function clearly has no analytic extension to the upper half plane. We locate the bound states at the solutions, in the upper half plane, of the equation $\xi^{18}+1=0$

$$\xi_j = \mathrm{e}^{\pi \mathrm{i}\frac{2j-1}{18}}, \quad j=1,\ldots,9. \tag{93}$$

For our first example, $q_1(t)$, we use as norming constants the residues of $(1+\xi^{18})^{-1}$ at these points. To six significant digits, these are:

$$\begin{aligned}\{&-0.054712-0.009647\mathrm{i}, -0.048113-0.027778\mathrm{i},\\ &-0.035710-0.042558\mathrm{i}, -0.019001-0.052205\mathrm{i},\\ &0.000000-0.055556\mathrm{i}, 0.019001-0.052205\mathrm{i},\\ &0.035710-0.042558\mathrm{i}, 0.048113-0.027778\mathrm{i},\\ &0.054712-0.009647\mathrm{i}\}.\end{aligned} \tag{94}$$

For our second example, $q_2(t)$, we use the same set of points $\{\xi_j\}$. For norming constants, we use instead the numbers, $\{C_j\}$, determined so that the L^2-error,

$$\int_0^\infty \left| f_d(t) - i\sum_{j=1}^{9} C_j \mathrm{e}^{\mathrm{i}\xi_j t}\right|^2 \mathrm{d}t, \tag{95}$$

is minimized. Here $f_d(t)$ is the inverse Fourier transform of $r_d(\xi)$, see Eq. (56). To six significant digits, these are

$$\begin{aligned}\{&-0.004027+0.005771\mathrm{i}, 0.021100-0.046418\mathrm{i},\\ &-0.153690+0.089410\mathrm{i}, 0.251055+0.037842\mathrm{i},\\ &0.000000-0.198290\mathrm{i}, -0.251055+0.037842\mathrm{i},\\ &0.153690+0.089410\mathrm{i}, -0.021096-0.046418\mathrm{i},\\ &0.004027+0.005771\mathrm{i}\}.\end{aligned} \tag{96}$$

Figs. 9A and B show $q_1(t)$ and $q_2(t)$, respectively. The transverse magnetization profiles they produce are shown in Figs. 9C and D.

Example 4. We consider 90° pulses with a variety of different choices for the bound states. We approximate the magnetization profile using the function $r_{18}(\xi)=\frac{1}{1+\xi^{18}}$. As before $\{\xi_j : j=1,\ldots,9\}$ denotes the poles of $r_{18}(\xi)$ in the upper half plane, see (93). We find the potentials that use the following collections of bound states:

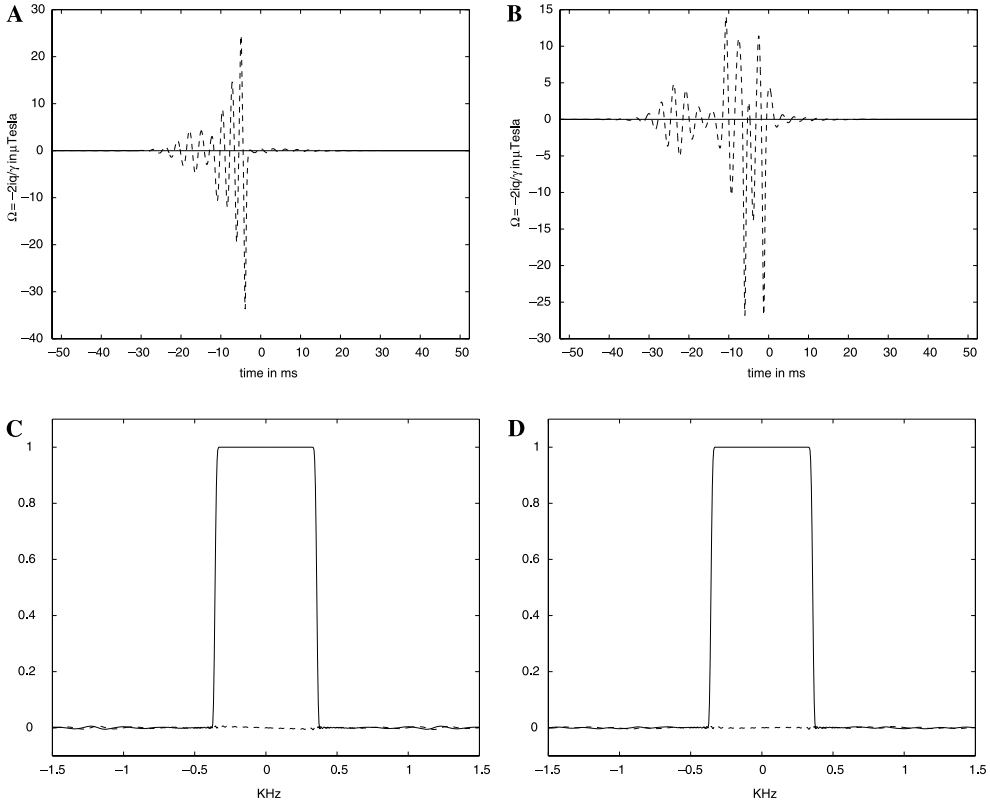

Fig. 9. Pulse profiles and corresponding transverse magnetization profiles for pulses with a piecewise polynomial reflection coefficient and some bound states. (A) The pulse profiles for $q_1(t)$. (B) The pulse profiles for $q_2(t)$. (C) The transverse magnetization produced by $q_1(t)$. (D) The transverse magnetization produced by $q_2(t)$.

$$\mathscr{B}_1^+ = \{\xi_1, \xi_9\}, \quad \mathscr{B}_2^+ = \{\xi_1, \xi_2, \xi_3, \xi_7, \xi_8, \xi_9\},$$
$$\mathscr{B}_3^+ = \{\xi_1, \xi_2, \xi_3, \xi_4, \xi_5, \xi_6, \xi_7, \xi_8, \xi_9\}, \quad \mathscr{B}_1^- = \{\xi_5\},$$
$$\mathscr{B}_2^- = \{\xi_3, \xi_4, \xi_5, \xi_6, \xi_7\} \tag{97}$$

The corresponding potentials are labeled $\{q_1^+(t), q_2^+(t), q_3^+(t), q_1^-(t), q_2^-(t)\}$. We use, for norming constants, the residues of $r_{18}(\xi)$ at the corresponding poles. With these choices, $q_3^+(t)$ is a self refocused pulse, supported in $(-\infty, 0]$. The left norming constants in this example are on the order of 10^7.

Each potential is computed at 2000 points and required less than 10 s to find on a 2 GHz Pentium Linux box. Fig. 10A shows the potentials $q_1^+(t), q_2^+(t)$, and $q_3^+(t)$. Fig. 10B shows the potentials $q_1^-(t)$ and $q_2^-(t)$ along with the minimum energy pulse, $q_0(t)$, for the reflection coefficient $r_{18}(\xi)$. The larger the index, the farther to the left the potential is supported, and the

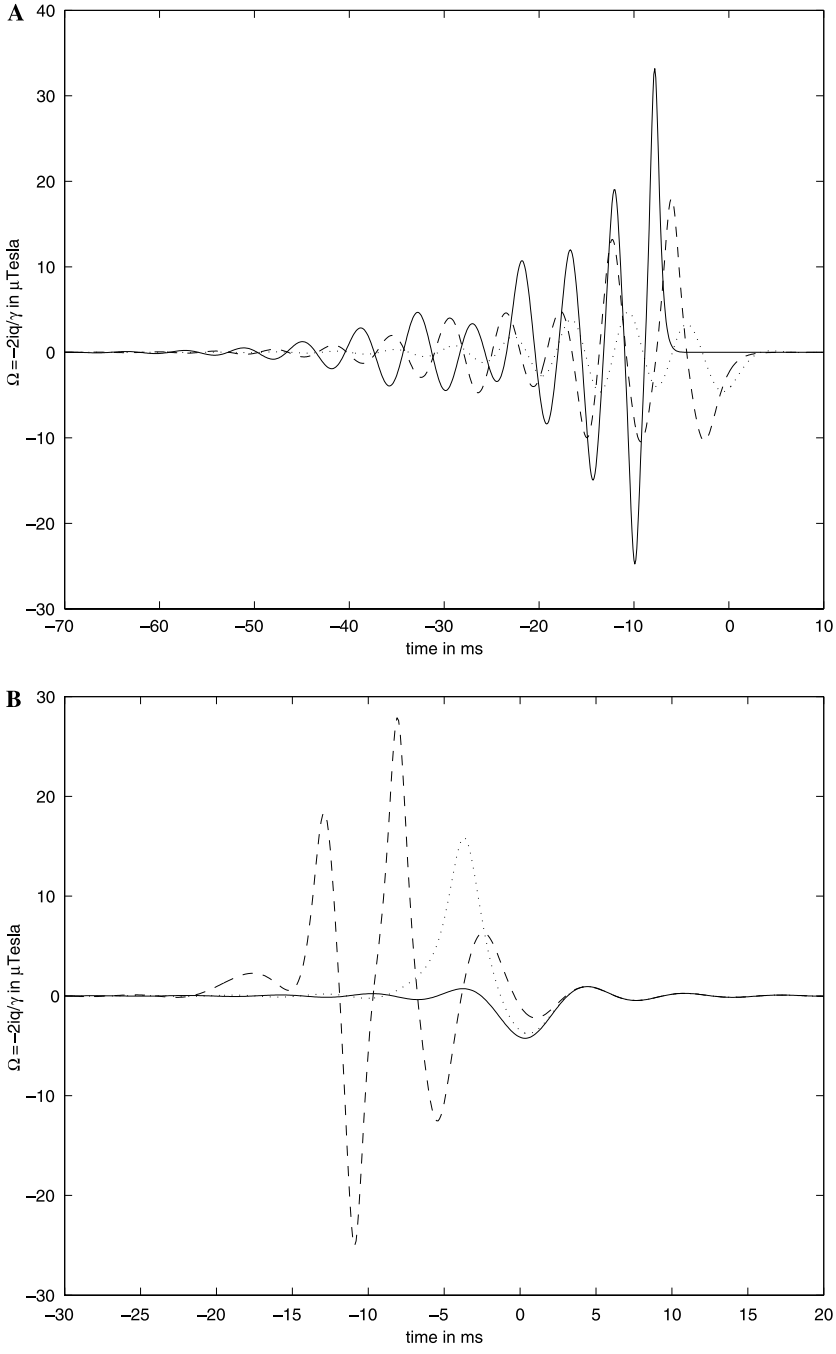

Fig. 10. Pulse profiles for a collection of pulses with the same reflection coefficient, $r_{18}(\xi)$ and different choices of bound states and norming constants. The greater the number of bound states, the larger the maximum amplitude. (A) The pulse profiles for $q_1^+(t)$ (dotted), $q_2^+(t)$ (dashed), and $q_3^+(t)$ (solid). (B) The pulse profiles for $q_1^-(t)$ (dotted), $q_2^-(t)$ (dashed), and $q_0(t)$ (solid).

larger the maximum amplitude. The magnetization profiles produced by these potentials are all close to the ideal. In Fig. 11A we show the magnetization profile for the minimum energy pulse $q_0(t)$, and in Fig. 11B, the magnetization profile for the self refocused pulse $q_3^+(t)$.

9.3. A wavelet example

For our final example we use a standard wavelet to define the x-magnetization. Such pulses were earlier constructed by several investigators using the SLR method; for a discussion and references see [13]. If $\psi(\xi)$ is a wavelet, then we set

$$m_1(\xi) = \psi(\xi),\ m_2(\xi) = 0,\ m_3(\xi) = \sqrt{1-\psi^2}. \tag{98}$$

Example 5 (*Mexican hat*). The Mexican hat wavelet is defined by the function

$$\psi(\xi) = \frac{4}{\sqrt{3\pi}}(1-\xi^2)\mathrm{e}^{-\frac{\xi^2}{2}}. \tag{99}$$

Fig. 12A shows the minimum energy IST pulse producing the transverse magnetization defined by $\psi(\xi)$, which is shown in Fig. 12B. In this example, the Marchenko equations were solved using simple iteration. The pulse took less than a minute to compute.

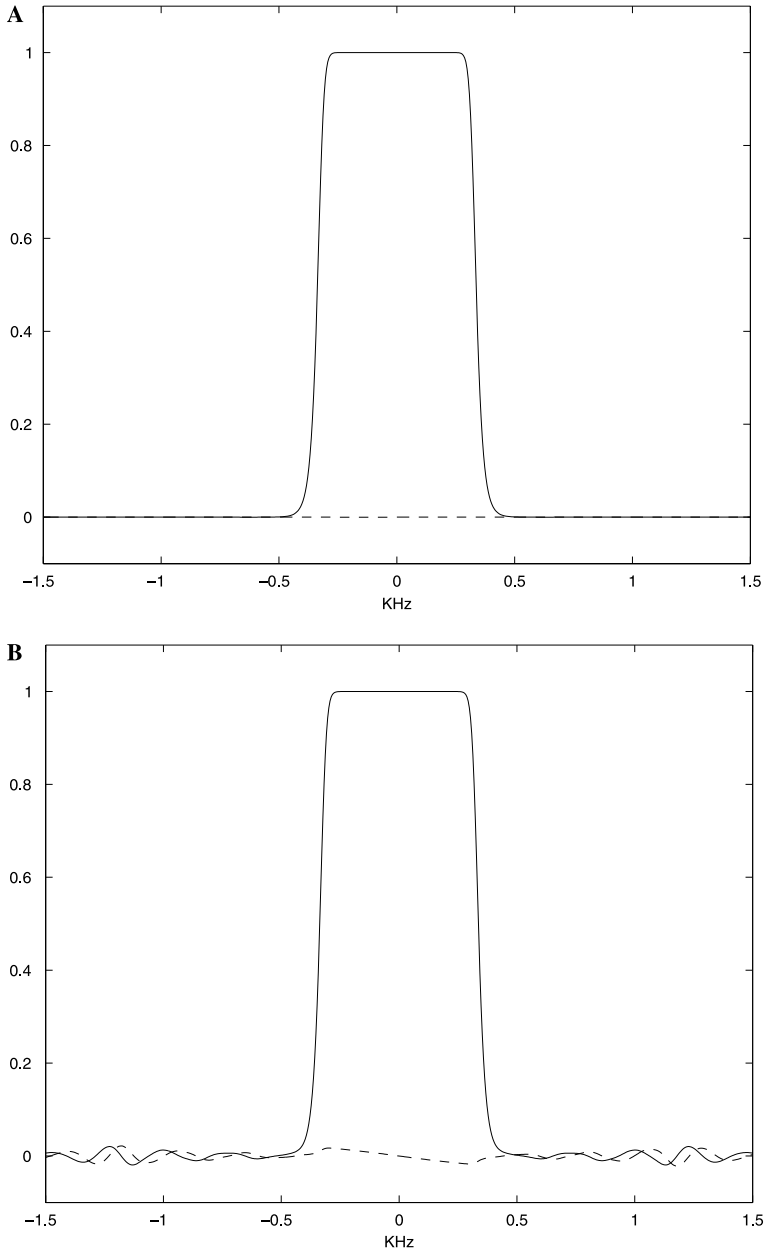

Fig. 11. The corresponding magnetization profiles for the two extreme cases: the minimum energy pulse and the self refocused pulse. (A) The transverse magnetization profile for q_0. (B) The transverse magnetization profile for q_3^+.

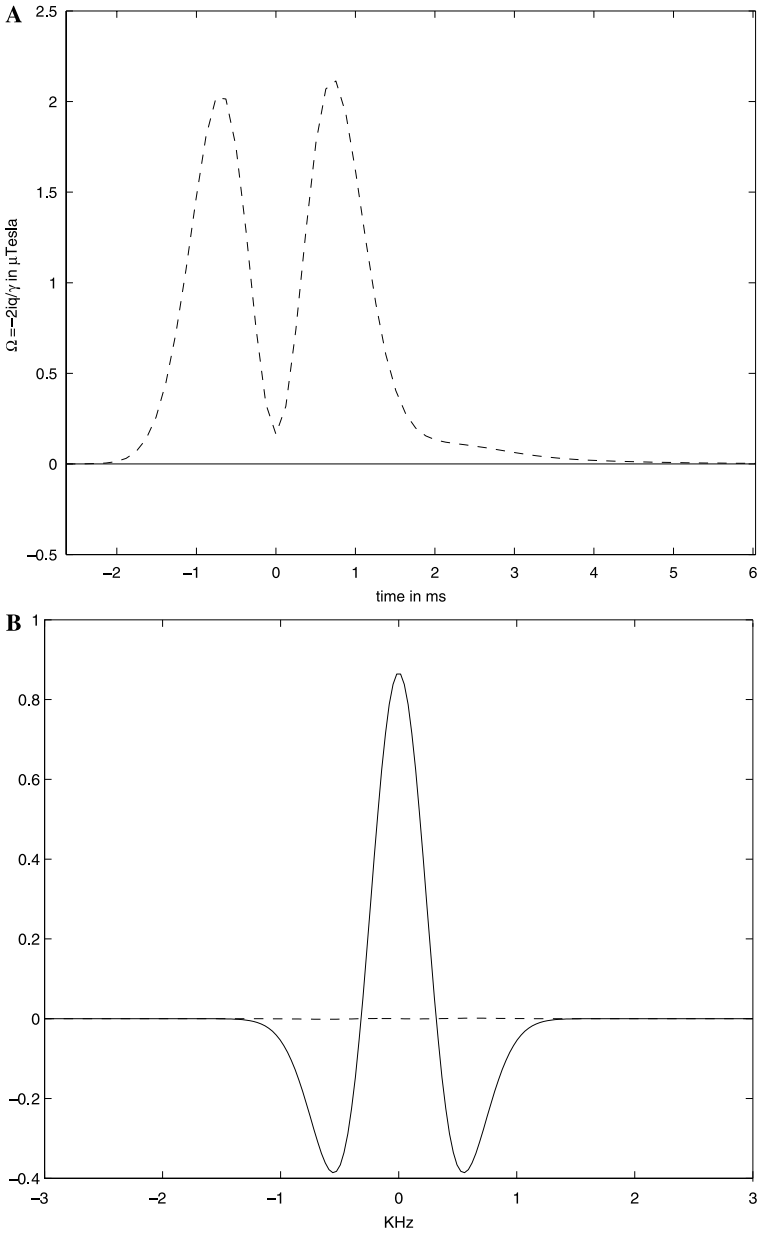

Fig. 12. A minimum energy pulse producing an excitation specified by the Mexican hat wavelet. (A) Minimum energy pulse. (B) Transverse magnetization profile.

9.4. A refocusing pulse

For our last example we construct a refocusing pulse. Ideally, an inversion pulse maps the equilibrium magnetization $[0,0,1]$ to the vector $[0,0,-1]$, for offset frequencies lying in a specified band. For each offset frequency, ξ, such a pulse defines an orientation reversing rotation $R(\xi)$ of the transverse plane. The pulse is a refocusing pulse if and only if this rotation is independent of the offset frequency, within the band where the longitudinal magnetization is inverted. Using the formulæ in Section (3), it is not difficult to show that an inversion pulse is refocusing if and only if $b(\xi)$ is real valued. This in turn implies that the pulse is symmetric. At the conclusion of such a pulse, the transformation, in-slice, of the transverse plane is a fixed reflection, e.g.

$$\begin{aligned} R_0 &: \begin{bmatrix} 1 \\ 0 \\ 0 \end{bmatrix} \rightarrow \begin{bmatrix} -1 \\ 0 \\ 0 \end{bmatrix}, \\ R_0 &: \begin{bmatrix} 0 \\ 1 \\ 0 \end{bmatrix} \rightarrow \begin{bmatrix} 0 \\ 1 \\ 0 \end{bmatrix}. \end{aligned} \tag{100}$$

Example 6. As shown in Section 4, it would require an infinite amount of energy, to exactly invert the magnetization for offset frequencies belonging to a band of positive length. For this reason we design a pulse which takes $[0,0,1]$ to $[\sin\epsilon,0,-\cos\epsilon]$, for a small, positive ϵ. It is not difficult to show that, if $b(\xi)$ is real, then, in-slice, this produces a family of orientation reversing rotations of the transverse plane of the form $r_\epsilon(\xi)R_0$, with $r_\epsilon(\xi)-\mathrm{Id}=\mathrm{O}(\epsilon^2)$. Fig. 13A shows a refocusing pulse designed to produce, in-slice, a 179°-flip of the equilibrium magnetization. Figs. 13B–D show the effects of this pulse on the x, y, and z components of the magnetization.

10. Conclusion

By introducing the left Marchenko equation, we obtain a method for finding RF-pulses with a given magnetization profile, and an essentially arbitrary choice of bound states. Using a very efficient implementation of this algorithm, obtained jointly with Jeremy Magland, we found several examples of RF-pulses with bound states. The main import of this algorithm is that it opens up the possibility of systematically studying the effects of bound states on the properties of an RF-pulse. We give a formula, due to Zakharov and Manakov, for the energy of an RF-pulse in terms of the magnetization profile and the locations of the bound states. Using this formula, and the inverse scattering method we determine the minimum energy RF-envelope that produces a given magnetization profile. The minimum energy profile is the one for which there are no L^2-bound states.

We obtain an estimate for the growth and decay of an RF-pulse in terms of the kernel functions appearing in the Marchenko equations. This estimate should prove useful in studying the relationships among the phase of the magnetization profile, the locations of bound states, and the support properties of the RF-envelope. Finally, we give an interpretation of the SLR-method, showing that it is, a special (singular) case of the IST approach. This analysis shows that the SLR design process trades direct control of the phase of the magnetization profile for the ability to specify the duration of a pulse. Through examples, we showed that the windowed IST pulse, comparable to an SLR pulse, has phase errors of

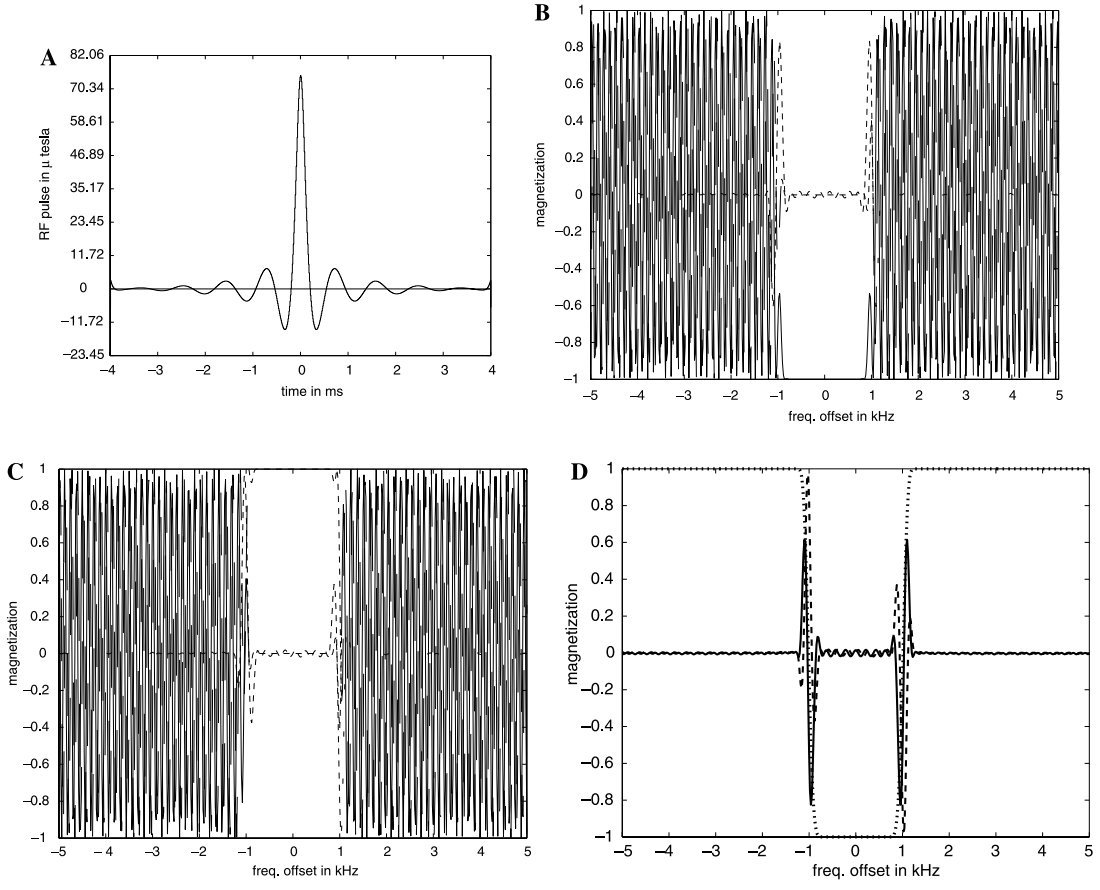

Fig. 13. A 2 kHz, minimum energy refocusing pulse designed to flip the equilibrium magnetization through 179°. The x-components are shown with a solid line, the y-components with a dashed line, and the z-components with a dotted line. Note the saturation, in (B, C), which occurs outside of the slice. (A) A minimum energy, selective refocusing pulse. (B) The effect of the pulse in (A) on the initial vector $[1,0,0]$. (C) The effect of the pulse in (A) on the initial vector $[0,1,0]$. (D) The effect of the pulse in (A) on the initial vector $[0,0,1]$.

a rather different character. In applications where control of the phase of the excitation is of paramount importance, the IST should prove to be a superior method.

Acknowledgments

I would like to thank Felix Wehrli for inviting me to visit the LSNI and giving me the opportunity to explore the world of magnetic resonance. I would also like to express my gratitude to Deans Samuel H. Preston and David Balamuth for supporting me in this endeavour. What I learned about MR in conversations with Felix, Peter Joseph, Steve Pickup, Hee Kwon Song, Branimir Vasilic and Alex Wright, has been indispensable in this work. Peter Joseph read through the entire manuscript and provided very helpful suggestions. I would also like to thank Carlos Tomei for all he has taught me over the years about inverse scattering. John D'Angelo provided some useful comments on the zeros of analytic functions. I would like to thank Jeremy Magland for his help with the numerical computations. Finally, I would like to thank the referees' for their very careful readings of an earlier version of this paper, and their many useful, and constructive suggestions.

Appendix A

A.1. The proof of Theorem 4

Assuming that $I_f(2t) < 1$, we need to show that the Marchenko equation

$$k_t(s) + \int_t^\infty \int_t^\infty f^*(s+y) f(y+x)\,\mathrm{d}y k_t(x)\,\mathrm{d}x = f^*(s+t), \tag{A.1}$$

can be solved by the iteration defined in (73), and the solution satisfies the estimate in (74). The proof is a simple induction argument. Clearly, for $t \leqslant s$, $|k_t^0(s)| \leqslant M_f(t+s) \leqslant M_f(2t)$. Assume that

$$|k_t^j(s)| \leqslant M_f(2t)\left[1 + I_f^2(2t) + \ldots I_f^{2j}(2t)\right]. \tag{A.2}$$

It follows from this assumption that:

$$|k_t^{j+1}(s)| \leqslant M_f(t+s) + M_f(2t)\left[1 + I_f^2(2t) + \ldots I_f^{2j}(2t)\right] \times \int_t^\infty \int_t^\infty |f^*(s+y) f(y+x)|\,\mathrm{d}y\,\mathrm{d}x. \tag{A.3}$$

As $s > t$, the induction hypothesis (A.2), with j replaced by $j+1$ follows easily from this estimate. Using a similar argument we can show that, for $j \geqslant 1$

$$\left|k_t^j(s) - k_t^{j-1}(s)\right| \leqslant M_f(2t) I_f(2t)^{2j}. \tag{A.4}$$

If $I_f(2t) < 1$, then this estimate shows that $\{k_t^j\}$ is a uniformly convergent sequence for $s \in [t, \infty)$. The limit, k_t^∞, is evidently a solution to (A.1). We can also pass to the limit in (A.2) to conclude that k_t^∞ satisfies (74).

A.2. Proof of Lemma 1

We use the Cauchy–Schwarz inequality to obtain

$$\begin{aligned}\|F_t h\|^2_{L^2([t,\infty))} &= \int_t^\infty \left| \int_t^\infty f(s+y) h(y)\,\mathrm{d}y \right|^2 \mathrm{d}s \\ &\leqslant \int_t^\infty \left[\int_t^\infty |f(s+y)|\,\mathrm{d}y \right. \\ &\quad \left. \times \int_t^\infty |f(s+y)||h(y)|^2\,\mathrm{d}y \right] \mathrm{d}s \\ &\leqslant I_f(2t) \int_t^\infty \int_t^\infty |f(s+y)||h(y)|^2\,\mathrm{d}s\,\mathrm{d}y \leqslant I_f^2(2t) \\ &\quad \times \int_t^\infty |h(y)|^2\,\mathrm{d}y. \end{aligned} \tag{A.5}$$

In the third and fourth lines we use the fact that $I_f(t)$ is a monotone decreasing function.

References

[1] M. Ablowitz, D. Kaup, A. Newell, H. Segur, The inverse scattering transform-Fourier analysis for nonlinear problems, Studies Appl. Math. 53 (1974) 249–315.
[2] R. Beals, R. Coifman, Scattering and inverse scattering for first order systems, CPAM 37 (1984) 39–90.
[3] R. Beals, P. Deift, C. Tomei, Direct and Inverse Scattering on the Line, American Mathematical Society, Providence, 1988.
[4] J. Carlson, Exact solutions for selective-excitation pulses, J. Mag. Res. 94 (1991) 376–386.
[5] J. Carlson, Exact solutions for selective–excitation pulses. II. Excitation pulses with phase control, J. Mag. Res. 97 (1992) 65–78.
[6] L. Faddeev, L. Takhtajan, Hamiltonian Methods in the Theory of Solitons, Springer Verlag, Berlin, Heidelberg, New York, 1987.
[7] F. Grünbaum, Concentrating a potential and its scattering transform for a discrete version of the Schrodinger and Zakharov-Shabat operators, Phys. D 44 (1990) 92–98.
[8] F. Grünbaum, A. Hasenfeld, An exploration of the invertibility of the Bloch transform, Inverse Probl. 2 (1986) 75–81.
[9] A. Hasenfeld, S.L. Hammes, W.S. Warren, Understanding of phase modulation in two-level systems through inverse scattering, Phys. Rev. A 38 (1988) 2678–2681.
[10] P. Le Roux, Exact synthesis of radio frequency waveforms, in: Proceeding of seventh annual meeting of the SMRM, 1988, p. 1049.
[11] G.B. Matson, An integrated program for amplitude-modulated rf pulse generation and re-mapping with shaped gradients, Mag. Res. Imag. 12 (1994) 1205–1225.
[12] H.E. Moses, R.T. Prosser, Eigenvalues and eigenfunctions associated with the Gel'fand–Levitan equation, J. Math. Phys. 25 (1984) 108–112.
[13] L.P. Panych, Theoretical comparison of Fourier and wavelet encoding in magnetic resonance imaging, IEEE Trans. Med. Imag. 15 (1996) 141–153.

[14] J. Pauly, P. Le Roux, D. Nishimura, A. Macovski, Parameter relations for the Shinnar–Le Roux selective excitation pulse design algorithm, IEEE Trans. Med. Imag. 10 (1991) 53–65.
[15] S. Pickup, X. Ding, Pulses with fixed magnitude and variable phase response profiles, Magn. Res. Med. 33 (1995) 648–655.
[16] S. Pickup, M. Popescu, Efficient design of pulses with trapezoidal magnitude and linear phase response profiles, Magn. Res. Med. 38 (1997) 137–145.
[17] D.E. Rourke, P.G. Morris, The inverse scattering transform and its use in the exact inversion of the Bloch equation for noninteracting spins, J. Mag. Res. 99 (1992) 118–138.
[18] D.E. Rourke, J.K. Saunders, A simple relationship between total RF pulse energy and magnetization response—The nonlinear generalization of Parseval's relation, J. Mag. Res., Ser. A 115 (1995) 189–196.
[19] M. Shinnar, L. Bolinger, J. Leigh, The synthesis of soft pulses with a specified frequency response, Mag. Res. Med. 12 (1989) 88–92.
[20] M. Shinnar, S. Eleff, H. Subramanian, J. Leigh, The synthesis of pulse sequences yielding arbitrary magnetization vectors, Mag. Res. Med. 12 (1989) 74–88.
[21] M. Shinnar, J. Leigh, The application of spinors to pulse synthesis and analysis, Mag. Res. Med. 12 (1989) 93–98.
[22] M. Shinnar, J. Leigh, Inversion of the Bloch equation, J. Chem. Phys. 98 (1993) 6121–6128.
[23] M.S. Silver, R.I. Joseph, D.I. Hoult, Selective pulse creation by inverse solution of the Bloch–Riccati equation, Magn. Reson. Med. 1 (1984) 294.
[24] M.S. Silver, R.I. Joseph, D.I. Hoult, Selective spin inversion in nuclear magnetic resonance and coherent optics, Phys. Rev. A 31 (1985) 2753–2755.
[25] W.S. Warren, Effects of arbitrary laser or NMR pulse shapes on population inversion and coherence, J. Chem. Phys. 81 (1984) 5437–5448.
[26] W.S. Warren, M.S. Silver, The art of pulse crafting: applications to magnetic resonance and laser spectroscopy, Adv. Mag. Res. 12 (1988) 247–384.
[27] V. Zakharov, L. Faddeev, Korteweg–de Vries equation, a completely integrable Hamiltonian system, Funk. Anal. Prilŏz. 5 (1971) 18–27.
[28] V. Zakharov, S. Manakov, On the complete integrability of the non-linear Schrödinger equation, Teor. Mat. Fiz. 19 (1974) 332–343.